RUHR UNIVERSITÄT BOCHUM

UNIVERSITY OF TWENTE.

Ruhr-University Bochum

Master Thesis

Wave Propagation In Granular Material: Theoretical And Numerical Analysis In Comparison To Experimental Data

Lisa de Mol

Mechanical Engineering

January 17, 2013

Supervisors

Prof. Dr.-Ing. H.Steeb

Continuum Mechanics
Ruhr-University Bochum

Prof. Dr. rer.-nat. S. Luding

Multi Scale Mechanics
University of Twente

Lisa de Mol, Matr.-Nr. 108007205053,
Ruhr-University Bochum, Mechanical Engineering
Supervisors:
Prof. Dr.-Ing. H.Steeb, Ruhr-University Bochum
Prof. Dr. rer.-nat. S. Luding, University of Twente
Bochum, January 17, 2013

Abstract

In this thesis wave propagation in granular material is investigated theoretically and numerically with the final goal to simulate experiments on ultrasonic wave propagation in a triaxial cell filled with glass beads in order to get better insight in the material behaviour. Studying wave propagation can answer fundamental questions concerning the material, since material moduli can be derived from wave properties. With numerical analyses not only a cheaper and easier way to realize parameter studies is chosen, but it has also the added value of offering information on the micro structure of the system, which is not possible in real physical experiments. The numerical algorithm on which all the simulations are based is the Discrete Element Method.

This work focuses on studying different numerical methods to calculate the wave velocity of a pressure wave and the compressional modulus of the material. A propagating wave is simulated to calculate the wave velocity once directly and once to obtain the dispersion relation by a Fourier analysis, which also gives information about the wave velocity. The compressional modulus is evaluated in another simulation that is based on the stress-strain relation of the material.

First regular granular systems (a 2D cubic, a 2D hexagonal, a 3D cubic and a 3D body centered cubic lattice) are analysed and the results from the numerical simulations compared to analytical solutions. From the comparison of the results, one can conclude that the chosen methods are reliable.

Later the investigations are concentrated on disordered granular systems, that resemble the physical experiments. The final results of these analyses cover a wide range of values with high deviations. The experimental results lie in this range. For future work an improvement of the presented methods is expected by slight modifications to reduce the deviations, which will make it possible to match the experiments better. The proposed improvements vary from creating a bigger sample for the simulations to a more careful analysis of the simulation's results.

Notations

Granular Material

ν	Poisson's ratio
Φ	porosity
Ψ	volume fraction
ρ	particle's density
ρ_{bulk}	material's density
σ	stress
ε	strain
E	Young's modulus
e	void ratio
M	compressional modulus

Simulation

Δt	time step interval
Δ	particle overlap
γ	damping coefficient
$\boldsymbol{\Delta}$	relative displacement vector
ϑ	damping ratio
m	particle mass

$\mathbf{C}$ stiffness tensor

$\mathbf{F}$ generalised force vector

$\mathbf{f}$ force vector

$\mathbf{M}$ generalised mass matrix

$\mathbf{n}$ contact normal

$\mathbf{S}^c$ contact stiffness matrix

c stiffness coefficient

E_{kin} kinetic energy

l_b branch vector

N_T number of time steps

r particle radius

T total simulation time

t_c collision time

u potential energy density

V Volume

$\ddot{\mathbf{x}}$ acceleration vector

$\dot{\mathbf{x}}$ velocity vector

$\mathbf{x}$ position vector

Waves

λ wave length

ω angular frequency

$\hat{\mathbf{U}}$ amplitude of generalised displacement vector

$\mathbf{k}$ wave vector

$\mathbf{U}$ generalised displacement vector

f	frequency
G	shear modulus
k	wave number
t_s	travel time
v_P	P-wave velocity
v_S	S-Wave velocity
v_{group}	group velocity
v_{phase}	phase velocity

Mathematics

$\cdot$	scalar product/ matrix product
∇	nabla operator
$\otimes$	dyadic product

Contents

Chapter 1

Introduction

This short introduction gives a motivation on why wave propagation in granular material is studied. It then outlines the content and goal of this thesis, followed by an overview of how the thesis is structured.

1.1 Motivation

Granular materials can be understood as an assembly of particles. They are omnipresent in nature and various technological applications. You can for example think of soils, snow, salt or different kinds of powders as a granular material. Reasons for studying and understanding these materials are to predict their behaviour in order to improve or influence them later. Possible investigation fields could for example be the study of avalanches or erosion, but also the transportation of sand or other materials in industrial environments. How waves propagate in granular materials is a fundamental question. It can give information about the material behaviour and help to determine material properties.

1.2 Thesis goal and overview

The goal of this thesis is the study of wave propagation in granular materials. For a better initial understanding waves in regular ordered systems are analysed first. Two different types of lattices in 2D and two in 3D are taken into account. Then a random system is created and waves are excited in this sample.
Different analytical and numerical analysis methods are used. Table 1.1 gives an overview over all the used analysis methods used in this thesis. The analytical methods can only

	Lattices	Random
analytical	Principle of virtual displacement Dispersion relation	
numerical	Hooke's law Wave Dispersion relation by Fourier transform	

Table 1.1: Analysis methods

be used in the ordered systems, whereas the numerical methods apply for both, ordered and random configurations.
With the validation of the analysis methods on the regular systems, the random system is created for a numerical comparison to experimental results on wave propagation from the laboratories of the Ruhr-University Bochum. Trying to model the experimental set-up, the simulation's aim is to gain further insight in the material behaviour in general and especially during wave propagation.
The simulations for the regular systems and all the post-processing applications are programmed in MATLAB. For the random system a version of a code called TRUBAL from the Aston University in Birmingham (1994) is used.

The thesis starts with chapter 2 by introducing the main properties of granular material and the Discrete Element Method (DEM), which is the algorithm used in the simulations. The chapter is completed by outlining the main theoretical basics on waves. The

five analysis methods (cf. tab. 1.1) are the topic in chapter 3. Chapter 4 deals with the regular systems. Every analysis method is treated separately. Attention is drawn to the exact adoption of the methods for the lattices. The results are presented and compared in the end. The disordered system is dealt with in chapter 5. A short section on the experiments is followed by a section on the creation of the random system. The three remaining analysis methods for the random systems are then analysed in depth and evaluated in the end. The thesis finishes in chapter 6 with a conclusion and recommendations for future work.

Chapter 2

Fundamentals on granular material and wave propagation

This chapter serves as a theoretical introduction to granular material and wave propagation. After the main properties of granular material are named, the Discrete Element Method is explained. This is the numerical method which all the simulations are based on. Then the wave properties, that are of further use, are shortly depicted.

2.1 Granular Material

Granular materials are large conglomerations of discrete macroscopic particles (cf. [12]). The particle systems consist of particles with diameters larger than one micron (cf. [10]). Common examples for these materials are sand, different kinds of powders, but also avalanches can be investigated in the field of granular matter. The study of these materials is important for different applications, such as mining, agriculture and construction. Geological processes, such as erosion, need to be understood better. Granular materials are also ubiquitous in the food industry.

As granular material has lot of different characteristics and properties, only the properties for the further understanding of this thesis are introduced. One important characteristic is the material's density. On the one hand the particles have their density ρ and on the other hand the material has a density, that is referred to as bulk density ρ_{bulk}. The bulk density is closely related the volume fraction ψ, the porosity ϕ and the void ratio e. The volume fraction describes the fraction of particle volume, whereas the porosity describes the fraction of void volume in the material. The void ratio is the void volume related to the particle volume. The three properties are computed by

$$\psi = \frac{V_{\text{particles}}}{V} \quad , \qquad \phi = \frac{V_{\text{voids}}}{V} \quad , \qquad e = \frac{V_{\text{void}}}{V_{\text{particles}}} \quad . \tag{2.1}$$

These three quantities describe the same physical property in a different way and can be related to each other in the following way:

$$\phi = 1 - \psi \quad \text{and} \qquad \phi = \frac{e}{1+e} \quad . \tag{2.2}$$

With the volume fraction and the particle's density the bulk density can be obtained by

$$\rho_{\text{bulk}} = \psi\, \rho \quad . \tag{2.3}$$

Granular materials are described on a micro-level by looking at single particles and their contacts. Thus the number of contacts is a valuable characteristic. The coordination number Z is defined as the average number of contacts per particle.

Additional information about the material can be requested by the number of rattlers. A rattler is a particle that is not in contact with other particles. Here contact is defined by two particles touching accompanied by the transmission of forces on each other.

As for every material a stress-strain relation can be captured in a constitutive equation. The general form of Hooke's law

$$\varepsilon_{ij} = \frac{1+\nu}{E}\sigma_{ij} - \frac{\nu}{E}\delta_{ij}\sigma_{kk} \tag{2.4}$$

$$\sigma_{ij} = \frac{E}{1+\nu}\left(\varepsilon_{ij} + \frac{\nu}{1-2\nu}\delta_{ij}\varepsilon_{kk}\right) \tag{2.5}$$

is a constitutive equation for isotropic materials (cf. [26]), where ν is the Poisson's ratio and E the Young's modulus.

Different material parameters are defined to cover the material's behaviour. In this thesis the difference between the Young's modulus E and the compressional modulus M needs to be clarified. The Young's modulus E is related to a stress-strain-relation with stress-free boundaries, whereas the compressional modulus M is calculated by setting the strains on the boundaries to zero. A compression in $\mathbf{e}_3$-direction means for the calculation of E, that $\sigma_{11} = \sigma_{22} = 0$ and equation (2.4) for $i = j = 3$ is simplified to

$$\sigma_{33} = E\varepsilon_{33} \quad . \tag{2.6}$$

The stress-free boundaries allow a dilation of the material in the other two directions $\mathbf{e}_{11}$ and $\mathbf{e}_{22}$. The relation between strain in the direction of compression and strain in the transversal direction is defined as the Poisson's ratio (cf. [24]):

$$\nu = -\frac{\varepsilon_{11}}{\varepsilon_{33}} = -\frac{\varepsilon_{22}}{\varepsilon_{33}} \quad . \tag{2.7}$$

The same compression with the boundary conditions $\varepsilon_{11} = \varepsilon_{22} = 0$ for the calculation of M leads with equation (2.5) to

$$\sigma_{33} = \frac{1-\nu}{(1+\nu)(1-2\nu)}E\varepsilon_{33} \quad . \tag{2.8}$$

Based on this relation the compressional modulus is defined as

$$M = \frac{1-\nu}{(1+\nu)(1-2\nu)}E \quad . \tag{2.9}$$

2.2 Discrete Element Method

The discrete element method (DEM) is a numerical algorithm used for the description of granular material behaviour. It is a method closely related to molecular dynamics (MD), but specially adapted to simulate the motion of macroscopic particles (cf. [11]). Based on Newton's equation of motion, the goal of a DEM-simulation is to describe the time-dependent positions and velocities of each single particle in a particle assembly, i.e. granular material.

A DEM-algorithm mainly consists of calculating all the forces acting on one particle and integrating the equations of motion to get the new positions and velocities per particle for the next time step. Alongside external forces on the material, the contact forces between particles play an important part in the force calculation procedure. Particle contacts are searched efficiently and their according contact forces determined.

Particles can be of diverse shapes. For simplicity disks are taken into account for the 2D case and spheres for the 3D case.

Each contact, that is found in one of the contact searching algorithms, is then regarded separately. One contact of particle i and particle j is illustrated in figure 2.1.

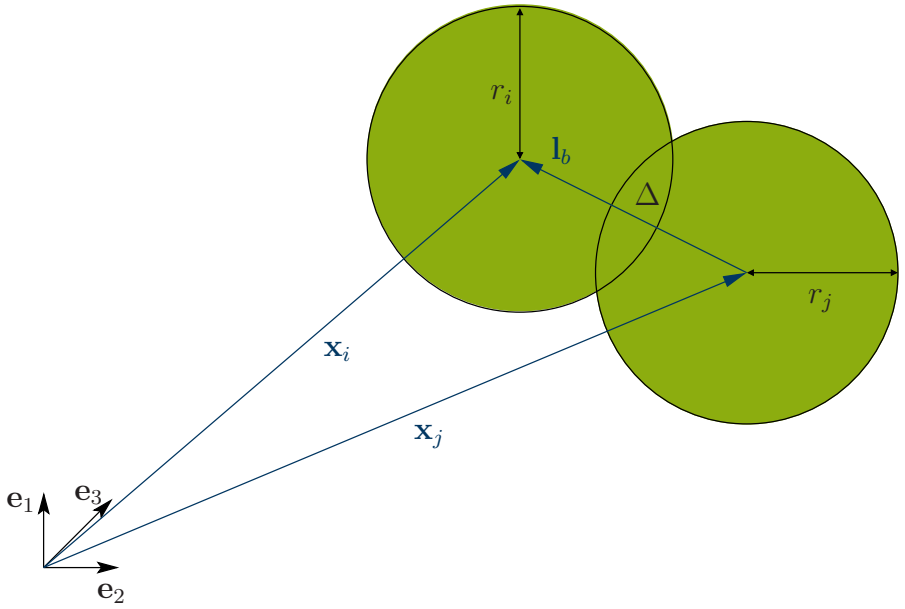

Figure 2.1: Schematic of two particles in contact

The particle's center of mass is given by the position vector $\mathbf{x}$ and the particles radius is r. A geometrically important quantity is the branch vector

$$\mathbf{l}_b = \mathbf{x}_i - \mathbf{x}_j \quad , \tag{2.10}$$

which is pointing on particle i from particle j. The contact normal direction $\mathbf{n}_{ij}$ is given by the normalized branch vector

$$\mathbf{n}_{ij} = \frac{\mathbf{l}_b}{|\mathbf{l}_b|} \quad . \tag{2.11}$$

For each two particles in contact the contact force is calculated. This can be done using various contact models, where the most common models are a linear model or a Hertzian contact model. In the linear case, particle interaction is modelled with a linear spring and dashpot. For a linear spring the force is calculated by the spring's stiffness coefficient c and the change in length of the spring. Translating this to particles the change of length is the particle overlap

$$\Delta = \mathbf{l}_b - (r_i + r_j)\,\mathbf{n}_{ij} \quad . \tag{2.12}$$

The dashpot contributes with the viscous damping coefficient γ and the relative velocity $\dot{\Delta}$ to the dissipative part of the force. The force from particle j on particle i is thus defined as

$$\mathbf{f}_{ij} = c\,\Delta\,\mathbf{n}_{ij} + \gamma\,\dot{\Delta}\,\mathbf{n}_{ij} \quad . \tag{2.13}$$

With the sum of all the forces on particle i excited by all the contacts C^P from particles j,

$$\mathbf{f}_i = \sum_{j=1}^{C^P} \mathbf{f}_{ij} \quad , \tag{2.14}$$

the acceleration at the current time step n is evaluated,

$$\ddot{\mathbf{x}}_i^{(n)} = \frac{\mathbf{f}_i^{(n)}}{m} \quad . \tag{2.15}$$

An appropriate integration scheme can now return the requested positions $\mathbf{x}$ and velocities $\dot{\mathbf{x}}$ at the next time step. The Verlet-integration scheme for example states

$$\mathbf{x}^{(n+1)} = 2\,\mathbf{x}^{(n)} - \mathbf{x}^{(n-1)} + \Delta t\,\ddot{\mathbf{x}}^{(n)} \tag{2.16}$$

$$\dot{\mathbf{x}}^{n} = \frac{1}{2\,\Delta t}\left(\mathbf{x}^{(n+1)} - \mathbf{x}^{(n-1)}\right) \quad . \tag{2.17}$$

To help estimating the parameters accurately, like the damping coefficient γ or the time step interval Δt, the collision of two particles is examined. This is resembled by two masses connected with a spring and a dashpot (cf. fig. 2.2), which are described by

$$m\ddot{\mathbf{x}} + \gamma\dot{\mathbf{x}} + c\mathbf{x} = 0 \quad . \tag{2.18}$$

An analytical solution for this problem is known and examined thoroughly in various

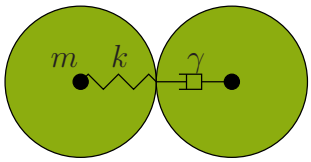

Figure 2.2: Schematic of two particles modelled as a damped oscillator

literature sources, e.g. [15]. The behaviour can be classified by defining a damping ratio

$$\vartheta = \frac{\gamma}{2\sqrt{c\,m}} \quad . \tag{2.19}$$

For $\vartheta < 1$ damped vibration can be observed, while for $\vartheta \geq 1$ the system is over-damped and does not oscillate. In the last case the motion is also referred to as aperiodic. Since for the DEM-simulation our system is required to show a damping behaviour, the damping ratio should be chosen according to the first case. This gives a limiting value for the damping coefficient:

$$\gamma < 2\sqrt{c\,m} \quad . \tag{2.20}$$

The time step interval Δt must be smaller than the collision time t_c, e.g. $\frac{1}{50}\,t_c$. The collision time is the time, in which two particles are in collision, or the time it takes for

the spring to get from its equilibrium length back to it. This equals half a period of full vibration and is expressed in (2.21).

$$t_c = \pi\sqrt{\frac{m}{c}} \tag{2.21}$$

Note that the collision time here is derived from the analytical solution of a simpler mass-spring system, not a mass-spring-dashpot system as described earlier. This was thought to be a convenient choice since t_c should give an upper limiting value for the time step interval and the period of a full vibration for a damped system is always larger than that of an undamped system.

To use a DEM-simulation sensible, not just these parameters have to be specified, but also initial and boundary conditions need to be set. Therefore information about the initial properties of the particles, i.e. radii, positions and velocities, is required. As boundary conditions one can restrict movement of some particles in a given direction or apply forces on them. A special type of boundary conditions are the periodic boundary condition. If you imagine a periodic box around the particles assembly, all the particles leaving the box at one side enter at the other side. So for example contacts between particles at the bottom of the system and the top of the system exist using this type of boundary conditions. They are used to simulate a particle assembly that represents a real system with much more particles in the periodic direction than actually needed in the simulation.

This presented simple DEM model can be extended further for different applications. In the case of particles with a rough surface for example friction forces have to be considered, too. In this case in addition to the spring in normal direction, springs in tangential direction are modelled for the frictional forces. A particle cannot be seen as a central force system any more. Thus the particle rotation gives one extra degree of freedom in 2D and three extra degrees of freedom in 3D. Other extensions or adaptations could also be the consideration of cohesive material behaviour.

2.3 Wave properties

A wave can be defined as the periodic propagation of a disturbance or oscillation through a medium (cf. [6]). It is primarily characterized by its frequency f, which is the repetition of oscillations per unit of time. Instead of the frequency f, often the angular frequency ω is used with the following relation:

$$\omega = 2\pi f \quad . \tag{2.22}$$

According to the frequencies, waves have different properties and are categorized. Waves with high frequencies are for example x-rays or light waves. Microwaves already do not have such high frequencies and sound waves even have comparably low frequencies at a range of $10^4 - 10^{10}$ Hz. The waves in this thesis can be assigned to the ultrasonic range. Apart from its frequencies the wavelength, the wave speed, the wave number, the wave vector and the propagation direction play an important role in describing waves.
The wavelength λ is the distance of a full oscillation period of the wave. Since the inverse of the frequency equals the time it takes the wave to perform one complete oscillation, the velocity of one phase, i.e. the phase velocity, can be computed by

$$v_{\text{phase}} = f\lambda \qquad . \tag{2.23}$$

Defining the wave number

$$k = \frac{2\pi}{\lambda} \tag{2.24}$$

and combining equations (2.22) and (2.23) another expression for the phase velocity states

$$v_{\text{phase}} = \frac{\omega}{k} \quad . \tag{2.25}$$

The phase velocity is used for non-dispersive media. Dispersion is the variation of phase velocity with frequency. If dispersion occurs it makes sense to look at the velocity the

envelope of the wave, i.e. the group velocity (cf. [3]), which is defined as

$$v_{\text{group}} = \frac{\partial \omega}{\partial k} \tag{2.26}$$

In non-dispersive media the group velocity equals the phase velocity. From now on, if the word wave velocity or wave speed is used, this refers to the group velocity. Generally the velocity can also be evaluated by looking at the time it takes for a signal to travel a certain length.

Regarding the propagation direction two main types of waves can be distinguished. If the propagation direction corresponds to the direction of oscillation, the wave is called longitudinal. Is the propagation direction perpendicular to the oscillation direction, the wave is called transverse. Longitudinal waves are also referred to as P-waves (pressure or compressional waves), whereas transverse waves are also called S-waves (shear waves). The propagation direction is mathematically captured in the wave vector $\mathbf{k}$. The wave vector's magnitude equals the wave number k.

The wave speed differs with the material the wave is travelling through. Knowing the speed of sound, one can calculate material properties, like the Young's modulus E, the compressional modulus M and the shear modulus G:

$$G = \rho_{\text{bulk}} v_S^2 \tag{2.27}$$

$$E = \rho_{\text{bulk}} v_P^2 \quad \text{or} \quad M = \rho_{\text{bulk}} v_P^2 \tag{2.28}$$

Here v_P is the speed of sound of a P-wave, v_S the speed of sound of a S-wave and ρ_{bulk} the system's density. The relation in equation (2.28) is valid for E or for M depending on the system. According to [23] $\rho_{\text{bulk}} v_P^2$ gives E in a bar and M in a system where the transversal length is larger than the length, in which the wave propagates. the systems in this thesis can be sorted to the last case. In a the post-processing steps of the simulations the compressional modulus M is calculated, not the Young's modulus E.

Mathematically wave motion, i.e. the displacement $\mathbf{U}$ at a certain time t and point $\mathbf{x}$ in

the material, is captured in the wave equation

$$\frac{\partial^2 \mathbf{U}(\mathbf{x},t)}{\partial t^2} = \mathbf{v}^2 \nabla^2 (\mathbf{U}(\mathbf{x},t)) \quad . \tag{2.29}$$

This equation can be solved analytically and its solution is called the harmonic wave solution, which reads

$$\mathbf{U}(\mathbf{x},t) = \hat{\mathbf{U}} \cdot \exp[i(\omega t - \mathbf{k}\cdot\mathbf{x})] \quad , \tag{2.30}$$

where $\hat{\mathbf{U}}$ is a vector that contains the amplitudes of displacement.

While working with waves, it can be useful to look at the time domain and the frequency domain. To switch between these different domains, mathematically the Fourier transform or the inverse Fourier transform is performed to go for example from the amplitude as a function of time to the intensity of the signal as a function of frequency. The Fourier transform is explained more thoroughly in chapter 3.5.

Chapter 3

Analysis methods

This chapter describes the five analysis methods used to get information about the wave speeds and material properties. The methods **Principle of virtual displacement** and **Hooke's law** directly lead to the calculation of the compressional modulus, whereas the methods **Dispersion relation**, **Wave propagation** and **Fourier transform** give information about the wave in the medium. With the obtained wave speed the compressional modulus can be computed. All five methods are applied on the regular systems in chapter 4 and three of them on the disordered systems in chapter 5.

3.1 Principle of virtual displacement

With the principle of virtual displacement the stiffness matrix for regular systems in 2D and 3D is derived. This derivation is extracted from [16]. Here the rotational degrees of freedom are neglected to model a frictionless system.
Regarding two particles i and j in contact and starting from the definition of particle overlap in normal direction,

$$\Delta = \mathbf{l}_b - (r_i + r_j)\,\mathbf{n}_{ij} \qquad , \tag{3.1}$$

a strain tensor ε with the change in length, which is the overlap, related to initial length can be defined:

$$\varepsilon = \frac{\Delta}{|\mathbf{l}_b|}\mathbf{n} \otimes \mathbf{n} \tag{3.2}$$

From the potential energy density u for one particle, with V as the volume of a unit cell,

$$u = \frac{1}{2V}\left(c\Delta^2\right) \quad , \tag{3.3}$$

the stress tensor σ and finally the stiffness tensor $\mathbf{C}$ can be calculated, according to (3.4).

$$\sigma_{\alpha\beta} = \frac{\partial u}{\partial \varepsilon_{\alpha\beta}} \quad , \quad C_{\alpha\beta\gamma\phi} = \frac{\partial \sigma_{\alpha\beta}}{\partial \varepsilon_{\phi\gamma}} \tag{3.4}$$

Applying Hamilton's principle of variation subjecting the system to a small deformation, thus varying the branch vector or overlap $\delta\mathbf{l}_b = \delta\Delta\mathbf{n}$, an expression for a single contact stiffness matrix is gained.

$$C_{\alpha\beta\gamma\phi} = \frac{|\mathbf{l}_b|^2}{V}\left(c\, n_\alpha n_\beta n_\gamma n_\phi\right) \tag{3.5}$$

This single contact stiffness matrix needs to be generalised. Therefore the averaging formula,

$$Q = \langle Q \rangle = \frac{1}{V}\sum_{p \in V} V^p Q^p \quad , \tag{3.6}$$

is used, where Q is any quantity that can be averaged over all particles p in an averaging Volume V. The relation for the stiffness tensor results in

$$C_{\alpha\beta\gamma\phi} = \frac{1}{V}\sum_{p \in V}\left(c\sum_{c=1}^{C}\frac{|\mathbf{l}_b|^2}{2} n_\alpha^c n_\beta^c n_\gamma^c n_\phi^c\right) \quad . \tag{3.7}$$

The sum regards one particle and each particle that is in contact with it. As volume the volume of a unit cell is to be chosen.

3.2 Dispersion relation

Dispersion describes a situation in which the phase velocity varies with frequency [6]. Regarding the definition given in equation (2.26) for the wave velocity as a function of the angular frequency and the wave number, the wave velocity for a certain wave length should equal the slope of a $k-\omega$-plot at the corresponding value of k. Investigating the dispersion relation of a material thus means finding a relation between the wave number and the angular frequency. From that relation the wave velocity can be derived and it can be differentiated whether the material behaves dispersive. If the relation is linear, the velocity does not change with the frequency, and the material is non-dispersive. Otherwise it is.

The dispersion relation for regular granular material is derived in [14]. The idea is to insert the harmonic wave solution in the DEM-Ansatz and solve it for the angular frequency ω with varying wave number k. Due to the periodicity of lattices in all directions only one particle and the ones in contact with it need to be regarded. The equation of motion for one particle p according to Newton's second law states

$$\mathbf{M}^p \cdot \ddot{\mathbf{U}}^p = \sum_q \mathbf{F}^{pq} \tag{3.8}$$

$\mathbf{M}$ is the mass matrix and $\mathbf{U}$ the generalized displacement vector. The force vector $\mathbf{F}^{pq}$ contains the sum of all contact forces on particle p. One contact force is calculated according to a linear spring model ($f = c\delta$). Here it is expressed by the matrix product of a contact stiffness matrix $\mathbf{S}^c$ and a relative displacement vector $\mathbf{\Delta}^c$.

$$\mathbf{M} \cdot \ddot{\mathbf{U}} = \sum_c \mathbf{S}^c \cdot \mathbf{\Delta}^c \tag{3.9}$$

All the vectors ($\mathbf{U}$, $\mathbf{F}^{pq}$ and $\mathbf{\Delta}^c$) and matrices ($\mathbf{M}$ and $\mathbf{S}^c$) differ with the number of degrees of freedom. The degrees of freedom change with the dimension (2D or 3D) and whether rotational particle motion is taken into account or not.

In the simplest case without a rotational degree of freedom the mass matrix is

$$\mathbf{M} = m\mathbf{I} \quad , \tag{3.10}$$

where $\mathbf{I}$ is the second order identity matrix for the 2D case and the third order identity matrix for the 3D case. The contact stiffness matrix reads

$$\mathbf{S}^c = c\,\mathbf{n}^c \otimes \mathbf{n}^c \tag{3.11}$$

and the relative displacement vector between particles q and p states

$$\boldsymbol{\Delta}^c = \mathbf{u}^q - \mathbf{u}^p \quad . \tag{3.12}$$

The displacements of each particle $\mathbf{u}$ are obtained by inserting the particles' positions into the harmonic wave solution (2.30). As position $\mathbf{x}$ for particle p a general value $\mathbf{x}^p$ is used, whereas the particles' q positions are dependent on that position with

$$\mathbf{x}^q = \mathbf{x}^p + 2r\mathbf{n} \quad . \tag{3.13}$$

Combining equations (2.30), (3.13) and (3.12), the displacement vector becomes

$$\boldsymbol{\Delta}^c = \hat{\mathbf{U}} \exp\left[i\left(\omega t - \mathbf{k}\cdot\mathbf{x}^p\right)\right](\xi - 1) \quad \text{with} \quad \xi = \exp\left(-ir\mathbf{k}\cdot\mathbf{n}\right) \tag{3.14}$$

Going back to the equation of motion, this results into the following eigenvalue problem:

$$\left(\bar{\mathbf{K}} - \omega^2\mathbf{M}\right)\hat{\mathbf{U}} = 0 \quad , \tag{3.15}$$

with

$$\bar{\mathbf{K}} = \sum \mathbf{S}^c\,(\xi - 1) \quad . \tag{3.16}$$

Solving it for a wave vector **k** in vertical direction with changing magnitude, $k-\omega$-plots can be obtained to analyse the dispersion relation.

Attention must be paid to the choice of wave numbers. The minimal and maximal wavelengths are restricted by the number of particles and their sizes. Figure 3.1 shows the minimal and maximal wave length for a chain of particles. If the particles are arranged differently, e.g. a non cubic lattice is chosen, the minimal and maximal wavelength need to be adapted to that special case. Hence it only makes sense to look at the dispersion

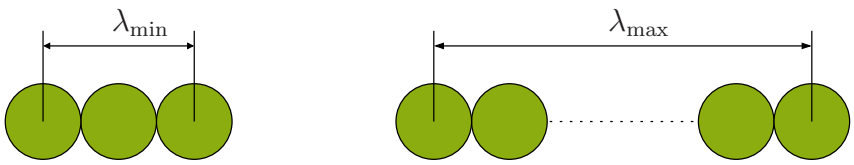

Figure 3.1: schematic to illustrate the minimal and maximal wavelengths

relation from a minimal wave number (maximal wave length) to a maximal wave number (minimal wavelength). The interval with which the subsequent wave numbers are determined, should be $\frac{k_{\min}}{2}$.

3.3 Hooke's Law

One way to determine compressional modulus of a granular material by DEM-simulation is based on Hooke's law. To be able to use Hooke's law correctly, the initial and boundary conditions have to be chosen properly: All the bottom particles' movement is restricted in horizontal direction, while all the top particles are subjected to a force in that same direction (cf. fig. 3.2). Periodic boundary conditions in horizontal direction are chosen to eliminate the influence of the system's size on the result.

The simulation time should be chosen such that the system is relaxed in the end, which means that the total kinetic energy of the system is dissipated.

In a post-processing step the compressional modulus M is computed. The periodic bound-

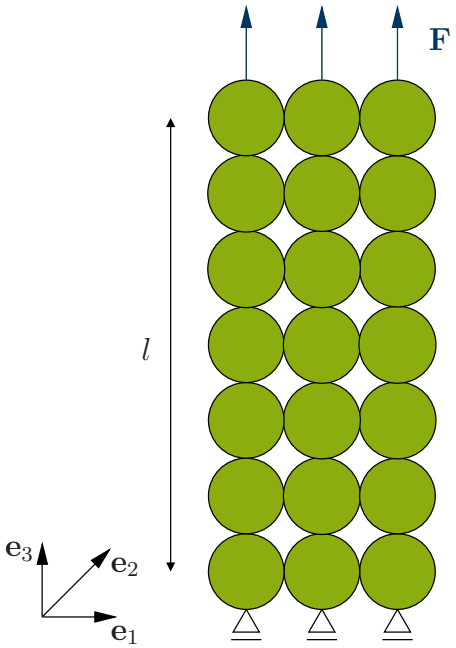

Figure 3.2: schematic of the boundary conditions for **Hooke's law** simulation

ary conditions resemble boundary conditions with the transversal strains set to zero. As described in chapter 2.1 the following equation is solved, if these boundary conditions apply to the system,

$$\sigma_{33} = M\,\varepsilon_{33} \quad . \tag{3.17}$$

The stress σ_{33} is the total force related to the area and the strain ε_{33} is the change in length related to the initial length (cf. (3.18)).

$$\sigma_{33} = \frac{F}{A} \quad , \qquad \varepsilon_{33} = \frac{\Delta l}{l} \tag{3.18}$$

Combining these expression the formula for the compressional modulus reads

$$M = \frac{F\,l}{A\,\Delta l} \tag{3.19}$$

Here the system's length l is known, F is known as the sum of all the applied forces on the top particles, the area A can be computed and the change in length is obtained from the results of the DEM-simulation.

3.4 Wave propagation

A way to determine the compressional modulus of a granular material by DEM-simulation is based on the calculation of the wave velocity. A P-wave, that propagates through the system, is simulated. To achieve this, the boundary and initial conditions are chosen as follows: The bottom particles' movement is restricted in horizontal direction, while all the particles in the second row get an initial velocity $\dot{\mathbf{x}}^{(0)}$ in vertical direction (cf. fig. 3.3). In horizontal direction the boundary conditions are periodic.

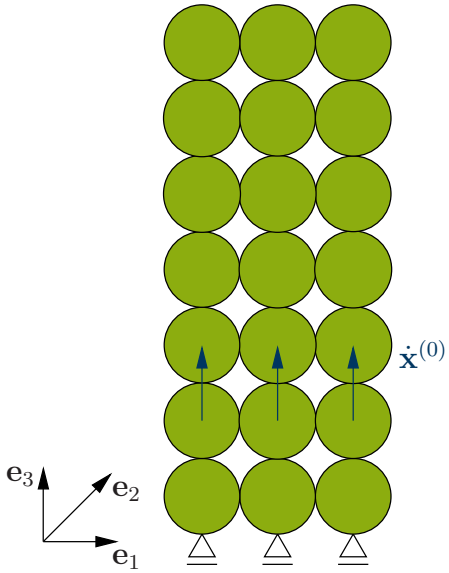

Figure 3.3: schematic of the boundary and initial conditions fot the **wave propagation** simulation

The simulation time should be chosen such that the excitation reaches the particles in the top layer.

The DEM-simulation results are used in a post-processing step to determine the wave speed. A good indication to measure the wave velocity needs to be established. This is discussed in chapter 4.

3.5 Fourier transform

The Fourier transform is a mathematical method to describe a function, that is given in time domain, in the frequency domain. The displacement or velocity as a function of time can be transformed to the signal's amplitude as a function of frequency. It gives information on how strong the signal is at a certain frequency. The general idea of the Fourier transform is that every function can be expressed as a Fourier series, meaning a sum of the trigonometric functions, where every summand contains frequencies and a coefficient that serves as weighting factor. Using this basic concept the Fourier transform $\mathcal{F}$ of a function $g(t)$ is defined as

$$\mathcal{F}\{g(t)\} = \int_{-\infty}^{+\infty} g(t) \exp(-i2\pi f t) \quad , \tag{3.20}$$

as stated in [5]. Here $g(t)$ is a continuous function. In most of the times however continuous functions are not available and one has to work with discrete values. In this case the discrete Fourier transform is used. According to the MATLAB function **fft** (cf. [2]) following formula is used for the discrete Fourier transform

$$X_k = \sum_{j=1}^{N} x_n \exp\left(-i2\pi \frac{k-1}{N}(j-1)\right) \tag{3.21}$$

The abbreviation **fft** stands for fast Fourier transform and means that the according algorithm is used. The results X_k are complex numbers. The absolute values of these complex numbers give the amplitudes, that are of interest.

In the case of a wave propagating through a granular material sample, every particle has a different amplitude for every time step. The amplitude is thus dependent on time and particle position. MATLAB offers a function **fft2**, that executes a fast Fourier transform for values that are dependent on two different parameters. The results, which are in the form of a matrix, can be visualized in a 3D plot. Scaling the output axes correctly, the initial axis of time transforms to an axis of frequency and the initial axis of particle

position transforms to an axis of wave number. The remaining axis gives the amplitude and thus the intensity of the signal. Choosing a convenient colour-code, that corresponds to the amplitudes, and looking in the frequency-/wave number-plane of the plot, the dispersion relation should be visible. At a certain position, for a certain time step, some frequencies are dominant. After the Fourier transform, the intensities of all the frequencies over the wave numbers are known. The frequencies with the highest amplitudes are the most dominant frequencies during wave propagation. They form the highest peaks in the plot and build a line that equals the dispersion relation.

Chapter 4

Regular Systems

This chapter starts by presenting the investigated lattices with all their properties. After shortly describing the adoption of all the previously explained analysis methods (cf. chapter 2) for these lattices, the results are given. The methods are evaluated critically and compared, in order to have a validated basis for the following investigation of random systems.

4.1 Lattices

A lattice, i.e. a crystalline structure, is characterized by periodicity on the microscopic level (cf. [4]). This means that the particles are arranged regularly in all directions. There are different ways to describe the geometrical properties of the periodic arrangements. In [18] the particle arrangement is for example described by point vectors. These are vectors from one particle to all the particles that are in contact with this chosen particle. Due to the regularity these vectors are the same independent from the chosen particle. Another way to describe a lattice is by defining a unit cell, which is a volume of space that can be translated in the directions of the point vectors without overlapping itself or leaving

voids (cf. [4]). There is no unique way to define a unit cell, although its volume is always the same regardless of its definition.

Two 2D and two 3D lattices are investigated. As 2D lattices a cubic and a hexagonal packing are chosen. Figure 4.1 shows a few particles to illustrate, how they are ordered.

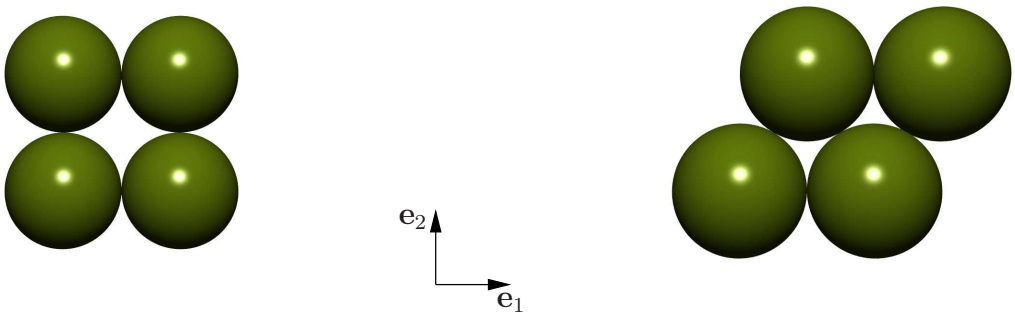

(a) Cubic (c) Hexagonal

Figure 4.1: 2D Lattices

As 3D lattices a simple cubic packing and body centred cubic packing are chosen (cf. fig. 4.2).

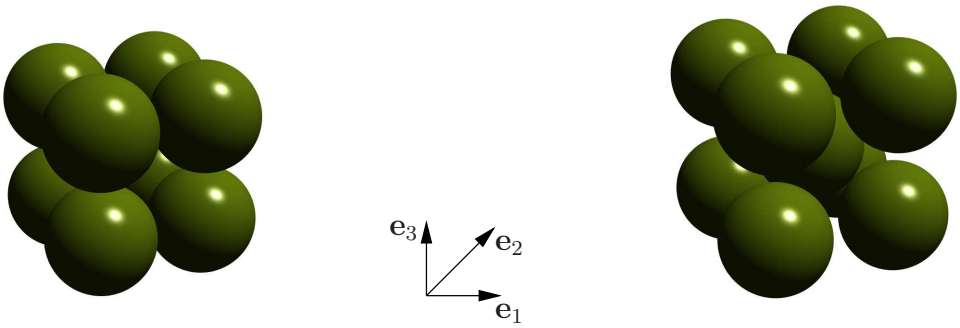

(a) Cubic (c) BCC

Figure 4.2: 3D Lattices

Additionally to the illustrations, the lattice structures are defined in table 4.1 by their points vectors. The point vectors correspond to the branch vectors $\mathbf{l}_b$. The branch vector has already been introduced in chapter 2.2.

Lattices do by definition not change the particle order under normal conditions. This means that they are characterized by a constant coordination number Z and a constant volume fraction ψ. The volume fraction can easily be calculated by dividing the particles'

	$\mathbf{l}_{b,1}$	$\mathbf{l}_{b,2}$	$\mathbf{l}_{b,3}$	$\mathbf{l}_{b,4}$	$\mathbf{l}_{b,5}$	$\mathbf{l}_{b,6}$	$\mathbf{l}_{b,7}$	$\mathbf{l}_{b,8}$
2D Cubic	$\begin{pmatrix}2r\\0\end{pmatrix}$	$\begin{pmatrix}0\\2r\end{pmatrix}$	$\begin{pmatrix}-2r\\0\end{pmatrix}$	$\begin{pmatrix}0\\-2r\end{pmatrix}$				
2D Hexagonal	$\begin{pmatrix}2r\\0\end{pmatrix}$	$\begin{pmatrix}r\\\sqrt{3}r\end{pmatrix}$	$\begin{pmatrix}-r\\\sqrt{3}r\end{pmatrix}$	$\begin{pmatrix}-2r\\0\end{pmatrix}$	$\begin{pmatrix}-r\\\sqrt{3}r\end{pmatrix}$	$\begin{pmatrix}r\\\sqrt{3}r\end{pmatrix}$		
3D Cubic	$\begin{pmatrix}2r\\0\\0\end{pmatrix}$	$\begin{pmatrix}0\\2r\\0\end{pmatrix}$	$\begin{pmatrix}-2r\\0\\0\end{pmatrix}$	$\begin{pmatrix}0\\-2r\\0\end{pmatrix}$	$\begin{pmatrix}0\\0\\2r\end{pmatrix}$	$\begin{pmatrix}0\\0\\-2r\end{pmatrix}$		
3D BCC	$\begin{pmatrix}\frac{2}{\sqrt{3}}r\\\frac{2}{\sqrt{3}}r\\\frac{2}{\sqrt{3}}r\end{pmatrix}$	$\begin{pmatrix}\frac{2}{\sqrt{3}}r\\\frac{2}{\sqrt{3}}r\\\frac{2}{\sqrt{3}}r\end{pmatrix}$	$\begin{pmatrix}\frac{2}{\sqrt{3}}r\\\frac{2}{\sqrt{3}}r\\\frac{2}{\sqrt{3}}r\end{pmatrix}$	$\begin{pmatrix}\frac{2}{\sqrt{3}}r\\\frac{2}{\sqrt{3}}r\\\frac{2}{\sqrt{3}}r\end{pmatrix}$	$\begin{pmatrix}\frac{2}{\sqrt{3}}r\\\frac{2}{\sqrt{3}}r\\\frac{2}{\sqrt{3}}r\end{pmatrix}$	$\begin{pmatrix}\frac{2}{\sqrt{3}}r\\\frac{2}{\sqrt{3}}r\\\frac{2}{\sqrt{3}}r\end{pmatrix}$	$\begin{pmatrix}\frac{2}{\sqrt{3}}r\\\frac{2}{\sqrt{3}}r\\\frac{2}{\sqrt{3}}r\end{pmatrix}$	$\begin{pmatrix}\frac{2}{\sqrt{3}}r\\\frac{2}{\sqrt{3}}r\\\frac{2}{\sqrt{3}}r\end{pmatrix}$

Table 4.1: branch vectors $\mathbf{l}_b$

area or volume, that fill the unit cell, by the total area (2D) or volume (3D) of a unit cell. The lattice properties coordination number Z, volume fraction Ψ and the system's density ρ_{bulk} are listed in table 4.2.

	Z	ψ	ρ_{bulk} $[\frac{\text{kg}}{\text{m}^3}]$
2D Cubic	4	$\frac{1}{4}\pi$	1570.80
2D Haxagonal	6	$\frac{1}{2\sqrt{3}}\pi$	1813.80
3D Cubic	6	$\frac{1}{6}\pi$	1047.20
3D BCC	8	$\frac{\sqrt{3}}{8}\pi$	1360.35

Table 4.2: lattice properties

For the simulations the size of the lattices needs to be defined. Therefore the number of particles np in each direction can be set. All the lattices have 200 particles in wave propagation direction $\mathbf{e}_2$ (2D) or $\mathbf{e}_3$ (3D). The 2D lattices have three particles in horizontal direction $\mathbf{e}_1$. The 3D lattices have four particles in the two horizontal direction $\mathbf{e}_1$ and $\mathbf{e}_2$. Since the particle order is not changed during simulation, the contacts are defined beforehand. Every contact is represented by a linear spring (wave propagation) or a linear spring-dashpot (Hooke's law). The lattices are simulated frictionless. Thus, tangential stiffness is not taken into account. The degrees of freedom are restricted to translational motion and do not regard rotational motion. The lattices are modelled as a mass-spring or mass-spring-dashpot system for the DEM simulation.
The particle and contact parameters used for the simulations are chosen in agreement with [19] and listed in table 4.3.

		2D lattices	3D lattices
r	[m]	0.001	
ρ	$[\frac{\text{kg}}{\text{m}^3}]$	2000	
k	$[\frac{\text{kg}}{\text{s}^2}]$	10^5	
γ	$[\frac{\text{m}}{\text{s}^2}]$	45	1.8
m	[kg]	$6.3\,10^{-3}$	$8.38\,10^{-6}$

Table 4.3: lattice parameters

4.2 Principle of virtual displacement

The formula for the calculation of the stiffness matrix (cf. (4.1)) was derived and explained in chapter 3.1 and can now be applied on all the chosen lattices.

$$C_{\alpha\beta\gamma\phi} = \frac{1}{V}\sum_{p\in V}\left(c\sum_{c=1}^{C}\frac{|\mathbf{l}_b|^2}{2}n_\alpha^c n_\beta^c n_\gamma^c n_\phi^c\right) \tag{4.1}$$

Since the other methods only compute the compressional modulus M, only the component that resembles this modulus is needed. According to the choice of coordinate system the component is C_{3333}. So a calculation of the total stiffness matrix $\mathbf{C}$ is not necessary. Intermediate results and final results of the computation for the compressional moduli M are presented in table 4.4.

	$\sum_{c=1}^{C}\mathbf{n}_1^c\mathbf{n}_1^c\mathbf{n}_1^c\mathbf{n}_1^c$	$\lvert\mathbf{l}_b\rvert$	V	M	
2D Cubic	2	$2\,r$	$(2\,r)^2$	100.00	kPa
2D Hexagonal	$\frac{9}{4}$	$2\,r$	$\frac{\sqrt{3}}{2}(2\,r)^2$	129.9	kPa
3D Cubic	2	$2\,r$	$(2\,r)^3$	50.00	MPa
3D BCC	$\frac{8}{9}$	$2\,r$	$4\sqrt{3}\,r^3$	25.66	MPa

Table 4.4: calculation of the compressional modulus M

Note that a unit cell is regarded. This means that only one particle with its contacts is taken into account. The sum over all the contacts is thus a sum from $c = 1$ until the coordination number Z. The volume V is the volume of the unit cell.

With

$$v_P = \sqrt{\frac{M}{\rho_{\text{bulk}}}} \tag{4.2}$$

the wave velocity is also calculated for comparison with the other methods. The results are listed in table 4.5.

	v_P $\left[\frac{\text{m}}{\text{s}}\right]$	M	
2D Cubic	7.98	100.00	kPA
2D Hexagonal	8.46	129.90	kPA
3D Cubic	218.51	50.00	MPa
3D BCC	137.34	25.66	MPa

Table 4.5: **Principle of virtual displacement** - Results

4.3 Dispersion relation

According to the derivation in chapter 3.2, where the harmonic wave solution was inserted in the DEM ansatz, the dispersion relation can be analysed by solving the following eigenvalue problem:

$$\left(\bar{\mathbf{K}} - \omega^2 \mathbf{M}\right) \hat{\mathbf{U}} = 0 \quad . \tag{4.3}$$

The matrix $\bar{\mathbf{K}}$ is obtained by a summation over all contacts, where the stiffness of each contact enters and also the wave vector $\mathbf{k}$. Equation (4.3) is solved for several different wave numbers k to get the dispersion curve $\omega(k)$. The variation of k is limited by a minimal and maximal wavelength λ (cf. chapter 3.2). These wavelengths differ per lattice. Table 4.6 gives an overview over these minimal and maximal values, with $np_{\mathbf{e}_3}$ as the number of particles in the direction of wave excitation and propagation.

The eigenvalues obtained from (4.3) correspond to the angular frequency ω, whereas the eigenvector $\hat{\mathbf{U}}$ gives information about the direction of oscillation, which is used to identify the type of wave, e.g. a P-wave or a S-wave.

Each degree of freedom gives an eigensystem, i.e. a pair of eigenvalue and eigenvector.

	$\lambda_{\min}$	$\lambda_{\max}$	$k_{\min}$	$k_{\max}$
2D Cubic	$4r$	$(np_{\mathbf{e}_3}-1)2r$	$\frac{\pi}{(np_{\mathbf{e}_3}-1)r}$	$\frac{\pi}{2r}$
2D Hexagonal	$2\sqrt{3}r$	$(np_{\mathbf{e}_3}-1)\sqrt{3}r$	$\frac{2\pi}{(np_{\mathbf{e}_3}-1)\sqrt{3}r}$	$\frac{\pi}{\sqrt{3}r}$
3D Cubic	$4r$	$(np_{\mathbf{e}_3}-1)2r$	$\frac{\pi}{(np_{\mathbf{e}_3}-1)r}$	$\frac{\pi}{2r}$
3D BCC	$\frac{4}{\sqrt{3}}$	$(np_{\mathbf{e}_3}-1)\frac{2}{\sqrt{3}}r$	$\frac{\sqrt{3}\pi}{(np_{\mathbf{e}_3}-1)r}$	$\frac{\sqrt{3}\pi}{2r}$
3D FCC	$\frac{4}{\sqrt{2}}r$	$(np_{\mathbf{e}_3}-1)\frac{2}{\sqrt{2}}r$	$\frac{\sqrt{2}\pi}{(np_{\mathbf{e}_3}-1)r}$	$\frac{\sqrt{2}\pi}{2r}$

Table 4.6: Minimal and maximal wave length and wave numbers

Plotting the eigenvalues ω versus the wave number k leads to plots with various branches. The number of branches corresponds to the degree of freedom, which is two for the 2D lattices and three for the 3D lattices since only translational motion is taken into account. Figure 4.3 shows the dispersion relation in the form of a ω-k-plot for the 2D lattices.

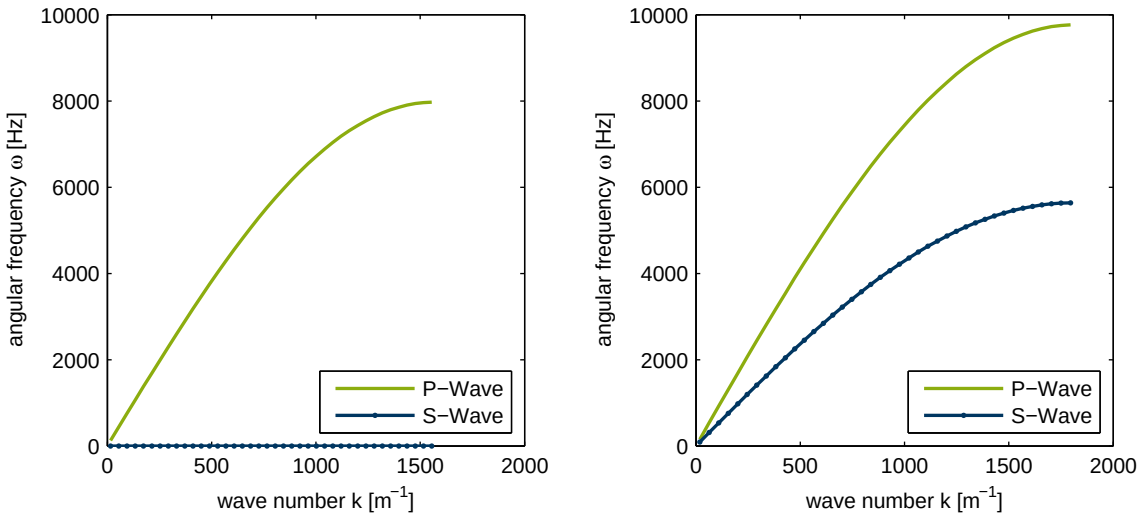

(a) Cubic lattice (b) Hexagonal lattice

Figure 4.3: 2D dispersion relation

Two branches can be distinguished for the cubic as well as for the hexagonal lattice. The eigenvectors allow to associate the upper branch with a P-Wave and the lower branch with a S-Wave for both lattices.

For the cubic lattice (cf. fig 4.3 (a)) the frequencies, that are assigned to a S-wave, are constant zero. This is to be expected with an excitation in vertical direction. Without friction the particles slide alongside each other and no oscillation except for the one in vertical direction is excited. The 2D cubic lattice reduces in its behaviour to a 1D chain.

However, for the hexagonal lattice (cf. fig 4.3 (b)) oscillations in the transverse direction can be observed additionally to the longitudinal oscillations of the P-wave. Due to the structure an excitation in vertical direction, also evokes oscillations in other directions. The frequencies increase linearly at small wave numbers, which mean large wave lengths. The results for the two different 3D lattices are displayed in figure 4.3.

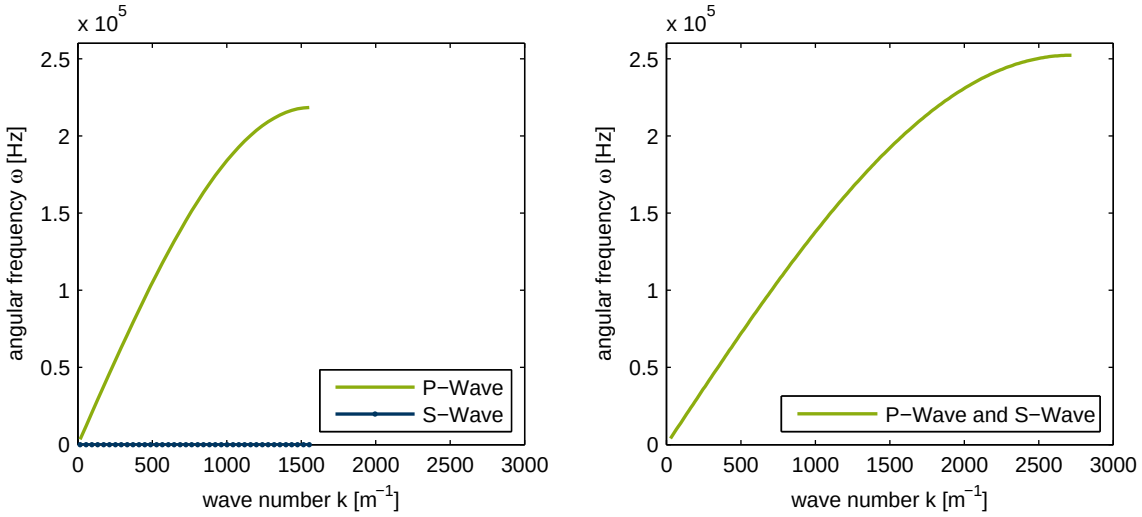

(a) 3D Cubic (b) 3D BCC

Figure 4.4: 3D dispersion relation

Since there are three degrees of freedom, three different angular frequency-lines are expected to be distinguishable. However, for the cubic lattice two of the computed eigenvalues are identical and for the BCC lattice all three eigenvalues have the same values. That is why only two branches can be distinguished in the ω-k-plots for the cubic lattice and only one can be detected for the BCC lattice.

The cubic lattice (cf. fig 4.4 (a)) shows symmetric behaviour in the two horizontal directions under excitation in vertical direction. Thus the motion in the translational degree of freedom in $\mathbf{e}_1$ and $\mathbf{e}_2$ should be the same. Indeed the particles oscillate in both directions $\mathbf{e}_1$ and $\mathbf{e}_2$ with an angular frequency of zero. The branch with the zero angular frequencies can be assigned once to a S-wave in the one vertical direction and once in the other vertical direction. The branch, that is different from zero, is assigned by its eigenvectors to a P-wave. The 3D cubic lattice also reduces to a 1D chain for the same reasons as for the 2D lattice. The dispersion relation for the 2D and 3D lattices are qualitatively exactly

the same. Quantitatively there is just a difference, because the 2D and 3D particles vary in their masses.

The BCC lattice (cf. fig 4.4 (b)) shows symmetric behaviour in all three directions under wave excitation in $\mathbf{e}_3$ direction. The particles are ordered in such a way that the collision with other particles arouse the same oscillations in the two vertical as well as in the horizontal direction. Thus the branch that can be assigned to the P-wave is the same as the two branches that are assigned to a S-wave in $\mathbf{e}_1$ and a S-wave in $\mathbf{e}_2$ direction.

One consistency check for the correctness of the general computation is done by the theoretical computation of the maximal angular frequency $\omega_{\max}$ according to equation (4.4).

$$\omega_{\max} = \frac{2\pi}{t_c} \tag{4.4}$$

The maximal angular frequency is determined for the cubic lattices only, because for these lattices t_c can be evaluated in the way described in 2.2. The values agree with the ones obtained by the dispersion relation.

As final results the slope at the maximal wavelength or the minimal wave number of the branch, that stands for the P-wave, gives the P-wave velocity v_P. With this velocity the material parameter M is computed as introduced in chapter 2.3.

The results can be extracted from table 4.7.

	v_P $[\frac{\mathrm{m}}{\mathrm{s}}]$	M	
2D Cubic	7.98	99.96	kPa
2D Hexagonal	8.46	129.85	kPa
3D Cubic	218.47	49.98	MPa
3D BCC	145.64	28.87	MPa

Table 4.7: **Dispersion relation** - Results

4.4 Hooke's law

The first method, that uses the DEM-method as basis, is the calculation of the compressional modulus M by Hooke's law. The simulations are conducted as described in chapter 3.3.

The final formula for the computation of M from chapter 3.3,

$$M = \frac{F\,l}{A\,\Delta l} \quad , \tag{4.5}$$

needs to be adapted to the 2D and the 3D lattices. In the 2D case the area A reduces to the system's length in horizontal direction, $l_{\mathbf{e}_1} + 2r$. In the 3D case the area A is the square that that is formed by all the particles in the $\mathbf{e}_1$-$\mathbf{e}_2$-plane. This is calculated by the product of lengths in these two directions

$$A = (l_{\mathbf{e}_1} + 2r)\,(l_{\mathbf{e}_2} + 2r) \quad . \tag{4.6}$$

Twice the radius is added to $l_{\mathbf{e}_1}$ and $l_{\mathbf{e}_1}$, because the lengths are measured from the particles center and the overlapping particles on the boundaries need to be taken into account, too.

The length l is the length in the direction of wave propagation $l_{\mathbf{e}_3}$. The length in wave propagation direction is measured from the bottom particle's position to the top particle's position. With the change in length Δl extracted from the simulation results the values listed in table 4.8 are obtained for the compressional modulus M. For comparison to the other methods the wave velocities are calculated by equation (4.2) and also listed in the table.

	v_P $[\frac{\mathrm{m}}{\mathrm{s}}]$	M	
2D Cubic	7.98	100.00	kPA
2D Hexagonal	8.47	130.09	kPA
3D Cubic	217.79	49.67	MPa
3D BCC	150.92	30.98	MPa

Table 4.8: **Hooke's law** - Results

4.5 Wave propagation

The second method, that uses the DEM-method as basis, is the calculation of the wave velocity v_P and the compressional modulus M by wave propagation. This method is investigated more thoroughly than the other methods, because it allows for a diversity of choices and assumptions.

The simulations are conducted as described in chapter 3.3.

The amplitude of the travelling wave should not influence the wave propagation. To be sure of this, the excitation velocity $\dot{x}^{(0)}$ is varied from $10^{-3} - 10$ $\frac{\mathrm{m}}{\mathrm{s}}$ and the resulting wave speeds are compared. Changing the initial velocity in this range has no noticeable influence on the wave speed of the cubic lattices. For the hexagonal and BCC lattice the wave speeds start to alter from an initial velocity $\dot{x}^{(0)} \geq 10^{-1}$ $\frac{\mathrm{m}}{\mathrm{s}}$. For this reason the following sections take only the results obtained with $\dot{x} = 0.01\frac{\mathrm{m}}{\mathrm{s}}$ into account.

As output the position vector $\mathbf{x}$ and the velocity vector $\dot{\mathbf{x}}$ for each particle and for every 10^{th} time step is written to a text file. These information can for example be used to determine the kinetic energy per time step n and particle i,

$$E^{(n)}_{\mathrm{kin},(i)} = \frac{1}{2} m \, \dot{\mathbf{x}}^{(n)}_{(i)} \cdot \dot{\mathbf{x}}^{(n)}_{(i)} \quad , \tag{4.7}$$

or the amplitude per time step n and particle i,

$$\hat{\mathbf{U}}^{(n)}_{(i)} = \mathbf{x}^{(n)}_{(i)} - \mathbf{x}^{(0)}_{(i)} \quad . \tag{4.8}$$

Figure 4.5 shows representatively the kinetic energy (cf. fig. 4.5(a)) and the amplitude (cf. fig. 4.5(b)) of one particle per layer plotted over time and initial particle position $x^{(0)}_{3(i)}$ for the 2D cubic lattice.

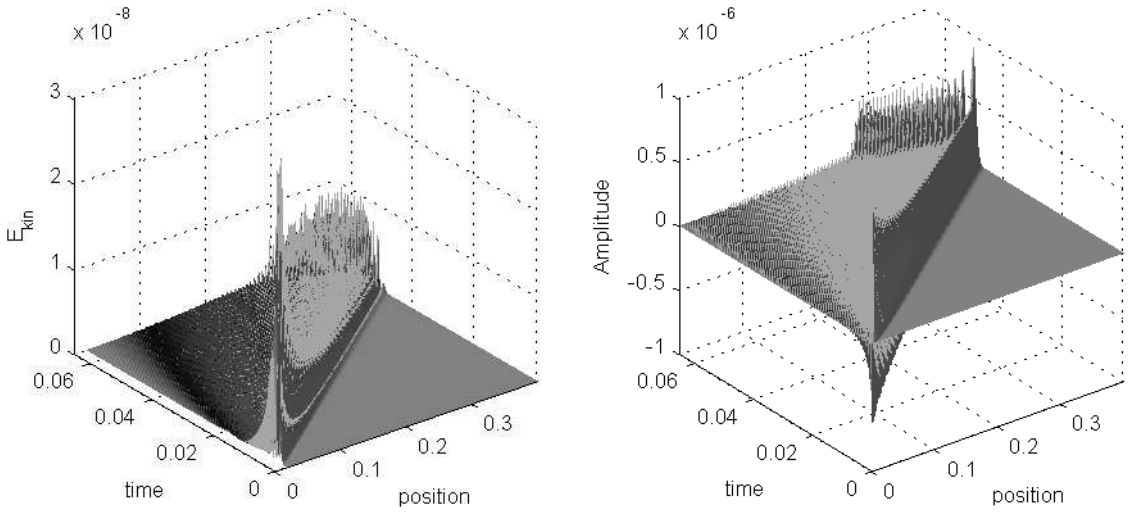

(a) Kinetic energy (b) Amplitude

Figure 4.5: Kintetic energy and amplitude over time and particle position of a propagating wave of the 2D cubic lattice

The travelling wave can be observed: The first particle in $\mathbf{e}_3$-direction is excited and has the highest initial kinetic energy or amplitude. It then transfers its motion to the next particles and the wave travels in excitation direction. So in time more and more particles farther away from the excitation source start to oscillate as soon as the wave reaches their position.

For the computation of the wave velocity the kinetic energy or the amplitude is used as an indication. The general idea is to look at the first peak in time of the kinetic energy or the amplitude in wave-direction of a chosen particle p and compare it to the corresponding peak of a reference particle p_{ref}. The peak is chosen as a measurement for the time, at which the wave has fully reached the particle for the first time. Dividing the initial distance of the two chosen particles by the difference in these two arrival times t_s, gives the P-wave speed v_P (cf. eq. (4.9)).

$$v_P = \frac{t_{s,(p)} - t_{s,(p_{\text{ref}})}}{x^{(0)}_{1,(p)} - x^{(0)}_{1,(p_{\text{ref}})}} \tag{4.9}$$

Intuitively one would choose the largest distance, i.e. a particle in the top layer with an excitation particle as reference. However, it is also considered that two particles somewhere between the bottom and top particle can be chosen. This has the advantage that probable influences from boundaries are limited, but the disadvantage that the assumption of a plane wave must be valid. Both methods are investigated with the kinetic energy and the amplitude. The method which considers a particle in the last layer and an excited particle as reference particle is labelled as method (1), while the method which considers two particles in between is referred to as method (2).

Exemplary, the kinetic energy and amplitudes in wave propagation direction for the chosen particles are shown in figure 4.6 for the 2D cubic lattice, which equals the 1D chain. The peaks are labelled with a red star (*).

Apart from the first peak, which is the reason for looking at these graphs, the magnitudes of the kinetic energies and amplitudes can be studied. The magnitudes of the excited particle are much higher than the magnitudes of the other particles. Then the magnitudes reduce the farther away the particle is from the source. The energy from one particle is not completely transferred to the next particle at once but distributed step by step over the whole lattice. The magnitudes of the particles in the last layer however increase again. This could be due to the boundary condition. Their movement in vertical direction is not restricted by boundaries and there are no particles above them which could limit this free movement.

These plots are looked at for all the four different lattices and the speed of sound computed according to equation (4.9). The results are listed in table 4.9.

	v_P $[\frac{\mathrm{m}}{\mathrm{s}}]$			
method	E_{kin} (1)	E_{kin} (2)	$\hat{\mathbf{U}}$ (1)	$\hat{\mathbf{U}}$ (2)
2D Cubic	7.92	7.97	7.85	7.91
2D Hexagonal	8.40	8.45	8.33	8.40
3D Cubic	216.97	218.41	214.98	217.05
3D BCC	144.70	145.63	143.35	144.59

Table 4.9: P-wave velocities calculated for the different methods

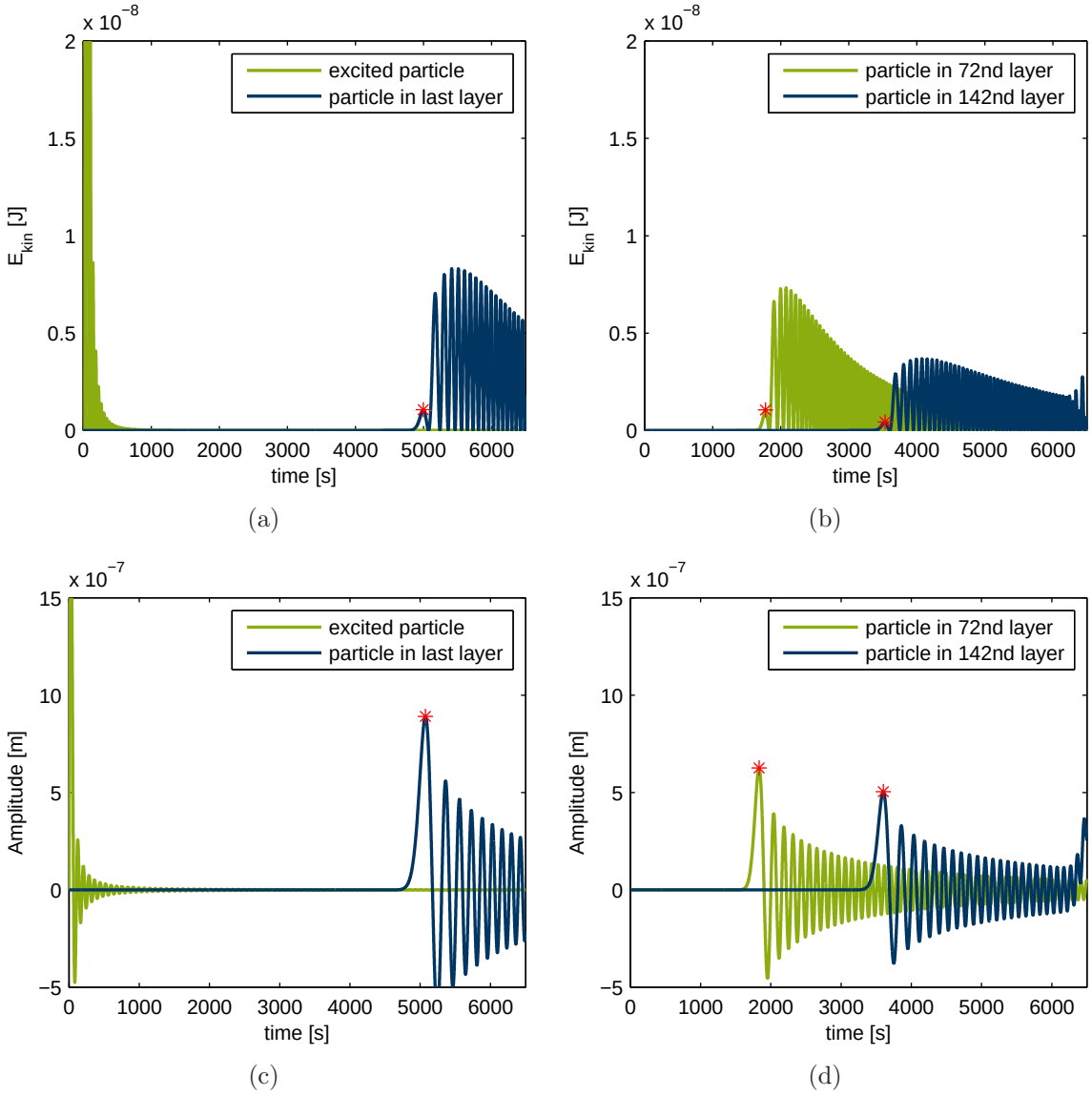

Figure 4.6: Kinetic energy and amplitudes of different particles of the 2D cubic lattice

For all the lattices the results of the different methods vary slightly, but in an acceptable range. Method (1) gives slower wave speeds than method (2) and looking at the amplitude instead of the kinetic energy also results in slightly slower wave speeds. Figure 4.7 shows the arrival times for the kinetic energy- and amplitude-peaks in dependence of the layer, where the corresponding particle is situated. Again the 2D cubic lattice is chosen representatively for all the other lattices, which show the same behaviour qualitatively. If the lines were completely linear, their slope would equal the wave speed. The line, which represents the amplitude, has a lower slope and thus leads to slower wave speeds. This is

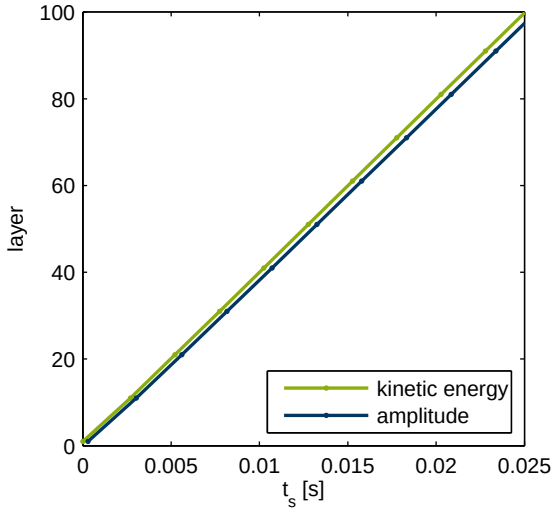

Figure 4.7: Arrival times for kinetic energy and amplitude method

in compliance with the numerical values in table 4.9. Another point, that can be noticed in the figure, is that the peak in kinetic energy is reached before the peak in amplitude. If a particle is excited by an initial velocity, its velocity is maximal directly in the beginning and then reduces, while the amplitude shows the opposite behaviour. This can also be explained by the conservation of energy. The velocity is the basis for the kinetic energy and the amplitude, which is the change in length of the springs in the DEM-simulation, the basis for the potential energy. In a conservative system, the sum of these two energies must be constant. An increase in the kinetic energy, must be accompanied by a decrease in potential energy and vice versa.

The reason for the difference in resulting wave speed between the kinetic energy and the amplitude, could lie in the changing excitation of movement of the particles during wave propagation. While the first particles are excited by an initial velocity, the other particles are excited by collisions with already oscillating particles. The oscillation changes its intensity, velocity and amplitude over time and is different for particles in different layers. The farther away the particles are from the excitation source, the earlier the kinetic energy reaches its maximum in comparison to the peak in amplitude.

Apart from the wave speed, the behaviour during wave propagation can be looked at with these simulations. The velocity vector is not combined in the kinetic energy, which is one scalar value, but each component is looked at separately. In the same way not only

the amplitude in wave propagation direction can be looked at, but each component is regarded. Since for the final results method (1) with the kinetic energy is chosen, the further demonstrations are restricted to the velocities of an excited particle and a particle in the last layer. Figures 4.8 and 4.9 show the velocity vector components of an excitation particle (green line) and a particle in the last layer (blue line) over time.

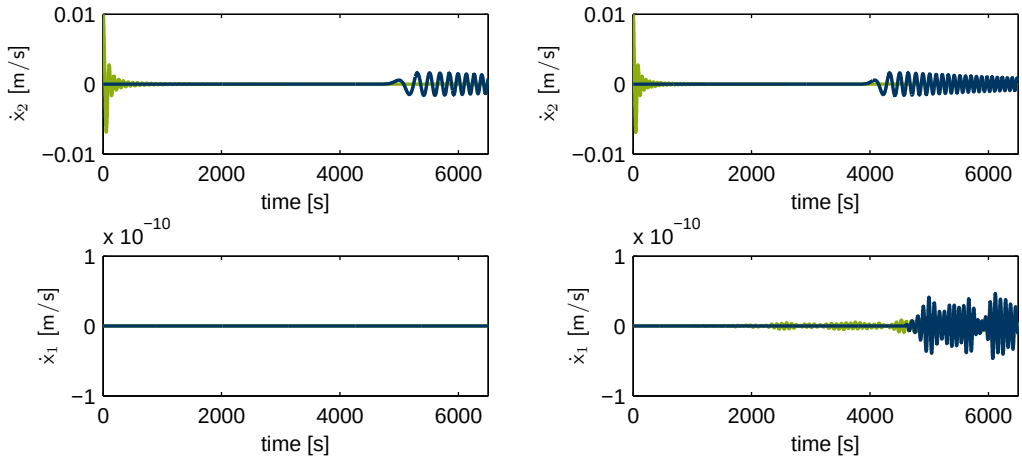

(a) 2D Cubic (b) 2D Hexagonal

Figure 4.8: Velocity components of the 2D lattices

The oscillation in excitation direction of the excited particle can nicely be observed. The particle in the last layer starts oscillating some time later as soon as the wave has reached its position.

A P-wave is excited and oscillations in wave propagation direction $\mathbf{e}_1$ expected. For the cubic lattices the velocity $\dot{x}_1$ oscillates around zero. The particles move back and forward. In the other directions the velocities $\dot{x}_2$ and $\dot{x}_3$ for the 3D lattices are zero. There really are only oscillations in $\mathbf{e}_1$-direction. This means that a clean P-wave propagates through the cubic lattices. This was already found out by looking at the dispersion relation (cf. chapter 3.2).

For the hexagonal lattice and the BCC lattice however, the velocities $\dot{x}_2$ (and $\dot{x}_3$) show values different from zero. Their magnitude is around $10^{-7} - 10^{-8}$ times smaller than the magnitudes of $\dot{x}_1$. Exciting a P-wave also arouses small oscillations of the particles in the transversal directions. They are so small that they could be numerical or referred to as

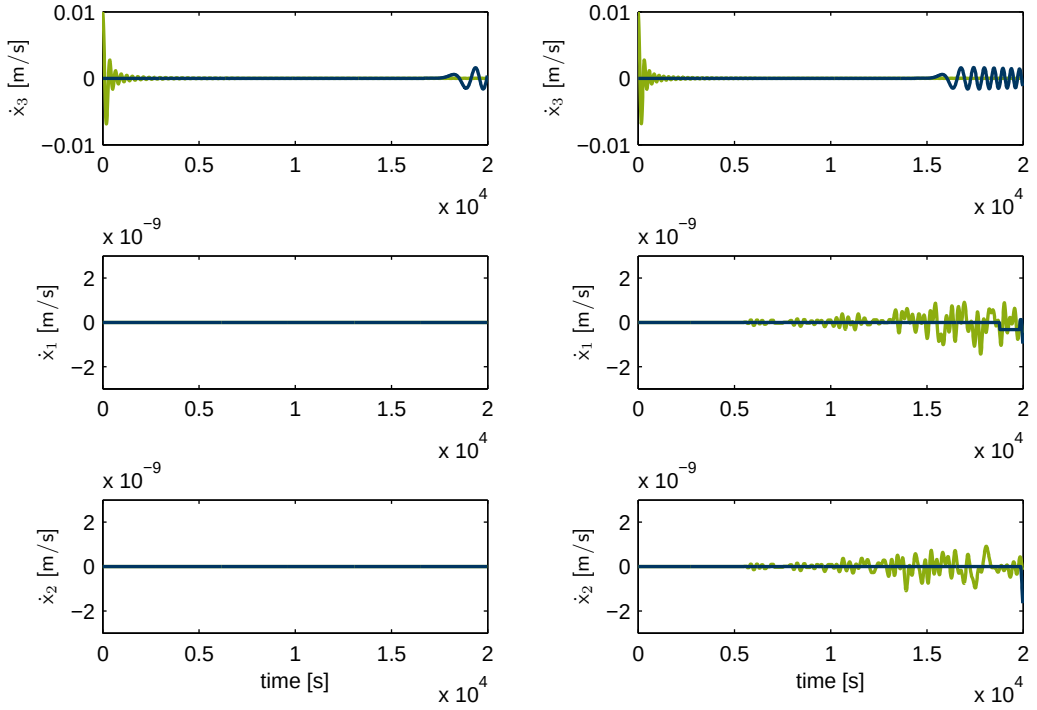

(a) 3D Cubic (b) 3D BCC

Figure 4.9: Velocity components of the 3D lattices

noise.

Although four different methods were used to calculate the wave speed and found to be consistent, only one method will be chosen to calculate the wave speed in a random system. Method (2), which means calculating the wave speed by looking at two particles somewhere in the lattice, is not suitable for random systems. In a random system the results are very much dependent on which particles are chosen. In contrary to the lattices, it also is not clear which effects occur in the system during wave propagation. Choosing an excitation particle as reference particle, reduces these insecurities and is expected to give better statistics. Another reason for choosing method (1) is, that it is considered to be closer to the experimental way of measuring the wave speeds. These aspects will be discussed later in chapter 5. Comparing the wave speeds obtained from method (1) for the kinetic energy and the amplitude in displacement to the results of the other analysis methods, the values for the kinetic energy are found to show the smallest deviation. So method (1) with the kinetic energy is chosen as the method for further use.

The wave speeds of the chosen method are listed in table and the compressional modulus

is added.

	v_P $[\frac{\mathrm{m}}{\mathrm{s}}]$	M	
2D Cubic	7.92	98.61	kPa
2D Hexagonal	8.40	128.09	kPa
3D Cubic	216.97	49.30	MPa
3D BCC	144.70	28.48	MPa

Table 4.10: **Wave propagation** - Results

4.6 Fourier transform

The Fourier transform is an alternative way to evaluate the dispersion relation. It requires the results of the wave propagation simulation. The displacement or velocity in wave propagation direction can be used, sorted by time step and lattice layer. The results shown in this chapter are obtained with the displacements.

After the Fourier transform (cf. chapter 3.5), one gets the amplitude in velocity or displacement in dependency on the wave number k and the angular frequency ω. To get the correct values the k and ω - axes need to be scaled. The wave number axis should have an interval of $\Delta k = k_{\min}$ from one value to the next, while the interval on the frequency axis is $\Delta\omega = \frac{2\pi}{T}$. The minimal wave number was already introduced for the different lattices in table 4.6. T is the total simulation time, which is either given or can be computed by the output time step interval and the number of time steps, via $T = \Delta t_{\text{output}}\, N_T$

Figures 4.10 and 4.11 show the results of the Fourier transform. The peaks form a line which matches the P-wave branch from the analytical calculation of the dispersion relation. This is a confirmation that the wave propagation simulation can be trusted. The wave propagation results lead to a comparable spectrum of the dispersion relation as the analytical calculation. The methods are consistent with each other. Only the P-wave branch is obtained. This is for once, because just the amplitudes in wave propagation direction were processed in the transform. Another reason is, that, if an S-wave propagates

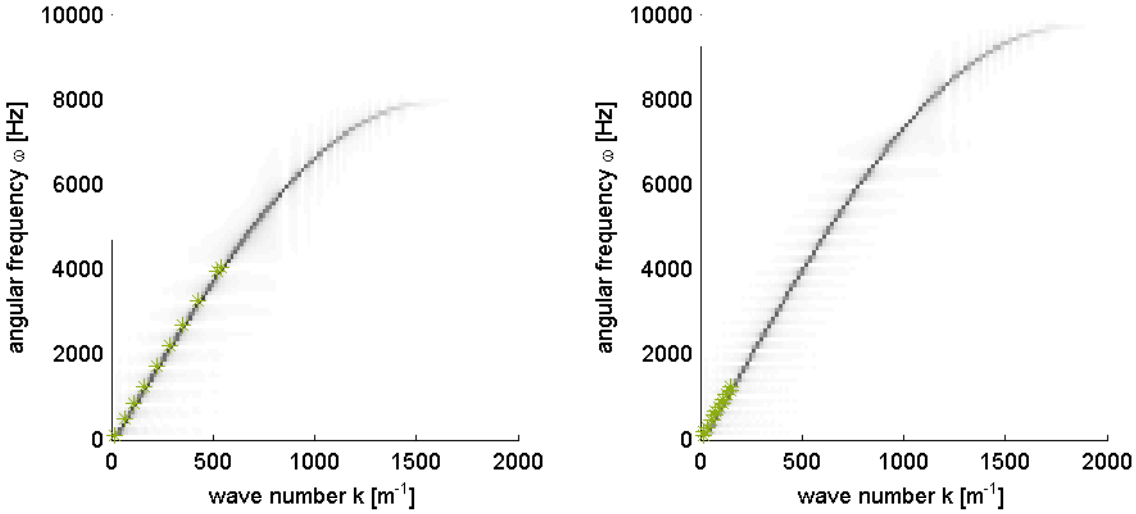

(a) Cubic Lattice (b) Hexagonal Lattice

Figure 4.10: Fourier transform of the 2D lattices

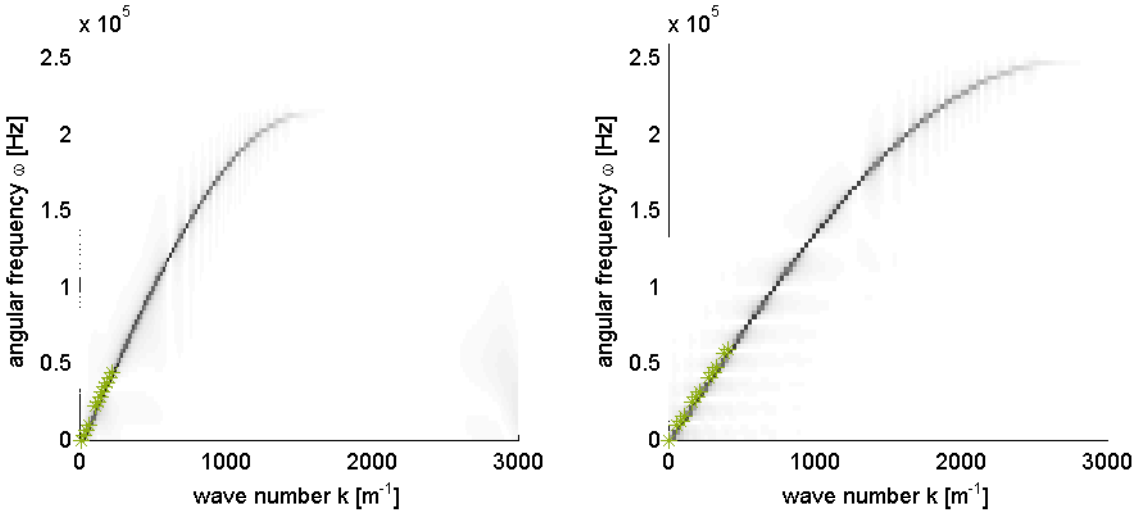

(a) Cubic Lattice (b) BCC Lattice

Figure 4.11: Fourier transform of the 3D lattices

in the system their amplitudes after the Fourier transform would be negligible small. The interpretation of the dispersion relation is already given in a previous chapter (cf. chapter 3.2).

Similarly to the analytical calculation of the dispersion relation, the wave speed can be obtained by calculating the slope in the linear regime. The green stars (*) in figures 4.10 and 4.11 show the chosen peaks, that are used for a linear fit. For every lattice 12 peaks where chosen. Less data points gave results that were deviating more. The obtained wave

speeds v_P and the corresponding compressional moduli M can be found in table 4.11.

	v_s^P $[\frac{\mathrm{m}}{\mathrm{s}}]$	M	
2D Cubic	7.60	90.82	kPa
2D Hexagonal	8.33	125.83	kPa
3D Cubic	218.61	50.05	MPa
3D BCC	144.58	28.44	MPa

Table 4.11: **Fourier transform** - Results

4.7 Comparison

Finally an overview over all the analysis methods is given. The results of the five methods, **Virtual displacement**, **Dispersion relation**, **Hooke's law**, **Wave propagation** and **Fourier transform** are listed in table 4.12.

For all lattices the agreement between the different methods is quite good. The **Fourier transform** gives for almost all the lattices values with the highest deviations from the other methods. This is probably due to the resolution which should be reduced to get exacter values. The method is still found to be important as it takes the **Wave propagation** simulation's results as input. So seeing a consistency between **Fourier transform** and the **Dispersion relation** confirms that the simulation is conducted correctly.

The **Wave propagation** is however influenced by different factors and there are different possibilities to excite a wave and extract the wave speed. The behaviour during wave propagation is studied for the regular systems and needs to be studied for the random systems in a similar way.

Due to the agreement in results and the separate investigation of all the analysis methods, all of them can be evaluated an appropriate way to get information about the wave velocity and the compressional modulus.

	Method	v_P $[\frac{m}{s}]$	M	
2D Cubic	Virtual displacement	7.98	100.00	kPa
	Dispersion	7.98	99.96	kPa
	Hooke	7.98	100.00	kPa
	Wave	7.92	98.61	kPa
	Fourier	7.60	90.82	kPa
2D Hexagonal	Virtual displacement	8.46	129.90	kPa
	Dispersion	8.46	129.90	kPa
	Hooke	8.47	130.09	kPa
	Wave	8.40	128.09	kPa
	Fourier	8.33	125.83	kPa
3D Cubic	Virtual displacement	218.51	50.00	MPa
	Dispersion	218.47	49.98	MPa
	Hooke	217.79	49.67	MPa
	Wave	216.97	49.30	MPa
	Fourier	218.61	50.05	kPa
3D BCC	Virtual displacement	137.34	25.66	MPa
	Dispersion	145.64	28.87	MPa
	Hooke	150.92	30.98	MPa
	Wave	144.70	28.48	MPa
	Fourier	144.58	28.44	kPa

Table 4.12: Overview over all methods

Chapter 5

Disordered System

This chapter deals with wave propagation and properties in randomly structured granular material. The DEM method is used to simulate previously conducted experiment with a polydisperse system of glass beads in a triaxial cell subjected to ultrasonic waves.
First the experimental setup and results are described in short. Then a way to model the experimental initial state numerically is proposed. With this initial state three analysis methods, which were thoroughly investigated in chapter 4, are presented and applied: **Wave Propagation**, **Hooke's law** and the **Fourier transform**. Finally the results of these three methods are compared with each other and to the experimental results.

5.1 Experiments

The experiments on wave propagation in a triaxial cell (cf. fig. 5.1) were conducted in the laboratories of the Ruhr-University Bochum by Emmerich (cf. [8]) and extended by Krause (cf. [13]). Glass beads from the manufacturer Mühlmeier GmbH (cf. tab. 5.1) are held together in a cylindrical geometry by a latex membrane. The pressure on the sample can be controlled hydraulically and is held constant. Waves are excited by an

ultrasonic transducer at one end of the sample and received on the other side. The time it takes for the wave to travel through the system is measured. Additional measurements are performed to gain information on the material, e.g. the volume fraction.

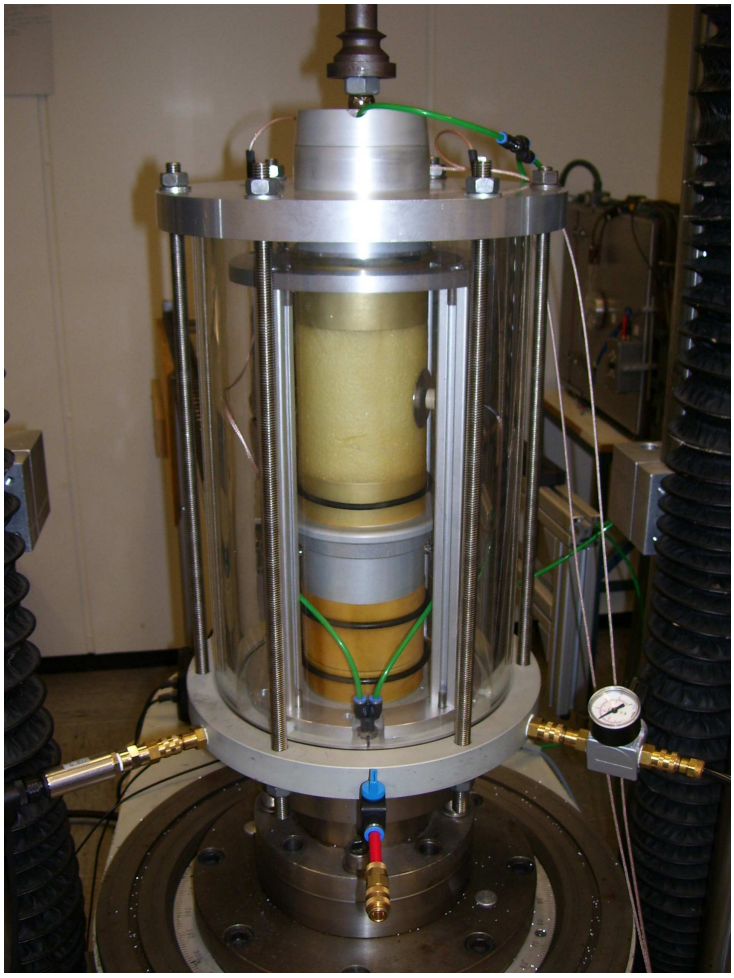

Figure 5.1: Triaxial cell, Ruhr-University Bochum, [8]

property		value	
producer		Mühlmeier GmbH & Co.KG	
name		Minibeads (glass beads)	
shape		round	
density	ρ	2500	$\frac{\text{kg}}{\text{m}^3}$
Young's modulus	E	59	GPa
Radii	r	0.40-0.50	mm

Table 5.1: Glass bead properties, [20]

The properties of the experimental setup are summarized in table 5.2. They serve as a

basis for the numerical simulation.

property		value	
axial length	l_a	109 - 117	mm
radial length	l_r	100	mm
pressure	p	1.95 - 2.00	bar
volume fraction	ψ	0.6267 - 0.6382	

Table 5.2: Experiments: initial state

With different initial states, the travel time of the ultrasonic waves through the sample is measured and related to the travel distance, i.e the axial length of the setup. The resulting wave speeds vary from $672 - 746 \frac{\mathrm{m}}{\mathrm{s}}$ for the initial state values from table 5.2.

5.2 Simulations with TRUBAL

The code used to simulate the disordered system is called TRUBAL (cf. [7]), a fortran code from the Aston University in Birmingham (1994). It is extended and changed over the years. To the last version of V.Magnanimo special features for wave propagation are added during this work. The DEM algorithm in TRUBAL is based on a Hertzian contact model, which is non-linear. Friction between particles is also implemented in contrast to the DEM code used for the regular systems. In agreement with the source code and various papers, that are based on simulations conducted in TRUBAL (cf. [25]), the forces in normal ($\mathbf{f}_n$) and tangential ($\mathbf{f}_t$) direction are calculated by

$$\mathbf{f}_n = \frac{2}{3}\frac{4G}{1-\nu} r^{\frac{1}{2}} \Delta^{\frac{2}{3}} \quad , \qquad \mathbf{f}_t = \frac{8G}{2-\nu} (r\Delta)^{\frac{1}{2}} (\Delta s) \quad . \tag{5.1}$$

Here r is the particle radius and Δ the normal overlap as defined in chapter 2.2. G and ν are the shear modulus and the Poisson's ratio of the particle material, respectively. The variable s is defined, such that the relative shear displacement between the two particles centers is $2s$ (cf. [25]).

The time step interval used for the simulations in TRUBAL is calculated inside the code and is dependent on the minimum particle mass and the maximum of the normal stiffness NO and the shear stiffness SH,

$$\Delta t = \frac{m_{\min}}{\max(NO, SH)} \quad . \tag{5.2}$$

A fraction of Δt is used. The value for this fraction is defined and changed during the simulation process.

For numerical reasons TRUBAL does not work with the SI-units. The scaling factors, that are needed to obtain from one TRUBAL unit the units in terms of SI-units are listed in table 5.3.

property	scaling factor	SI-unit
length	10^{-5}	m
mass	10^{-12}	kg
time	$\sqrt{10^{-17}}$	s

Table 5.3: Simulation parameters

The simulation parameters are given in table 5.4 in the units TRUBAL uses and takes as input values.

property		trubal value
particle radius	r	40-50
particle density	ρ	2.5
shear modulus	G	2.46
Poisson's ratio	ν	0.2
normal stiffness	NO	12.29
shear stiffness	SH	10.93

Table 5.4: Simulation parameters

The particle's densities and radii are matched with the experimental properties. The Poisson's ratio for the glass beads is not given by the manufacturer and is chosen to be 0.2 out of empirical reasons. With the relation between shear modulus G, Poisson's ratio

ν and the given Young's modulus E (cf. [24]),

$$G = \frac{E}{2\,(1+\nu)} \quad , \tag{5.3}$$

G is roughly estimated. The normal and tangential stiffness are just used for the calculation of the time step and not of further interest.

5.3 Initial state

For the numerical description of the experimental setup a system of 2000 randomly positioned particles is created. So only a part of the complete cell is modelled, which seemed to be sufficient to obtain reliable results and information about the system. An elongated rectangle is created to simulate the experimental setup's center. Periodic boundary conditions in all directions are chosen. The initial state copies the experimental pressure, volume fraction and glass bead properties. Polydispersity is realized by choosing particles with three different radii, $r_1 = 0.4$ mm, $r_2 = 0.45$ mm and $r_3 = 0.5$ mm. They are distributed equally, which means that 667 particles have the radius r_1 and r_3 and 666 particles the radius r_2.

The code TRUBAL provides a method to place particles in a prescribed box randomly. Initially the particles do not touch each other and there are thus no contact forces between them. One can then compress the box until the desired volume fraction and pressure. This is done within two steps. After a first compression until the volume fraction is almost reached, the system is relaxed and then compressed again accompanied by controlling the pressure. Relaxing means letting the energy dissipate out of the system. This results in a pressure of zero. The pressure p is the mean over the stresses in all three directions

$$p = \frac{1}{3}\,(\sigma_{11} + \sigma_{22} + \sigma_{33}) \tag{5.4}$$

For an isotropic stress state $p = \sigma_{11} = \sigma_{22} = \sigma_{33}$. The total stress in TRUBAL is calculated by averaging the dyadic product of contact forces $\mathbf{f}$ and the branch vector $\mathbf{l}_b$ over all the contacts c and particles p in the total volume V,

$$\sigma = \frac{1}{V} \sum_{p \in V} \sum_{c}^{C^p} \mathbf{f}^c \otimes \mathbf{l}^{pc} \quad , \tag{5.5}$$

where C^P is the number of contacts per particle.

The method of stress control works by correcting the strain to get closer to the requested stress. The strain correction is limited by an absolute maximum value. The process of compression, relaxation and another compression to reach the requested volume fraction and pressure is conducted frictionless. The friction is set to zero to get the particles closer together more easily. As soon as the volume fraction and pressure is reached friction is switched on with a value of $\mu = 0.3$ and the system is relaxed, while the pressure is controlled.

The evolution of volume fraction, pressure, coordination number and number of rattlers is monitored during the initial state creation and the plots shown in figure 5.2.

In all plots the two compression steps can be detected. The pressure, the coordination number and the volume fraction increase during compression, whereas the number of rattlers decreases. During the first relaxation an intermediate equilibrium is reached. After the second compression the volume fraction and the pressure rise to the desired values. All the parameters converge at the final relaxation. An equilibrated state is obtained.

For further investigations and better statistics two more initial states are created altering only the random positions of the particles in the beginning of the initial state creation. An overview over the most important properties of these three initial states can be found in table 5.5. Figure 5.3 shows the initial state of sample (1). The different colors stand for the different radii of the particles (r_1 = green, r_2 = blue, r_3 = black). Note that the length of the sample is just a fraction of 0.28 of the experimental sample's length.

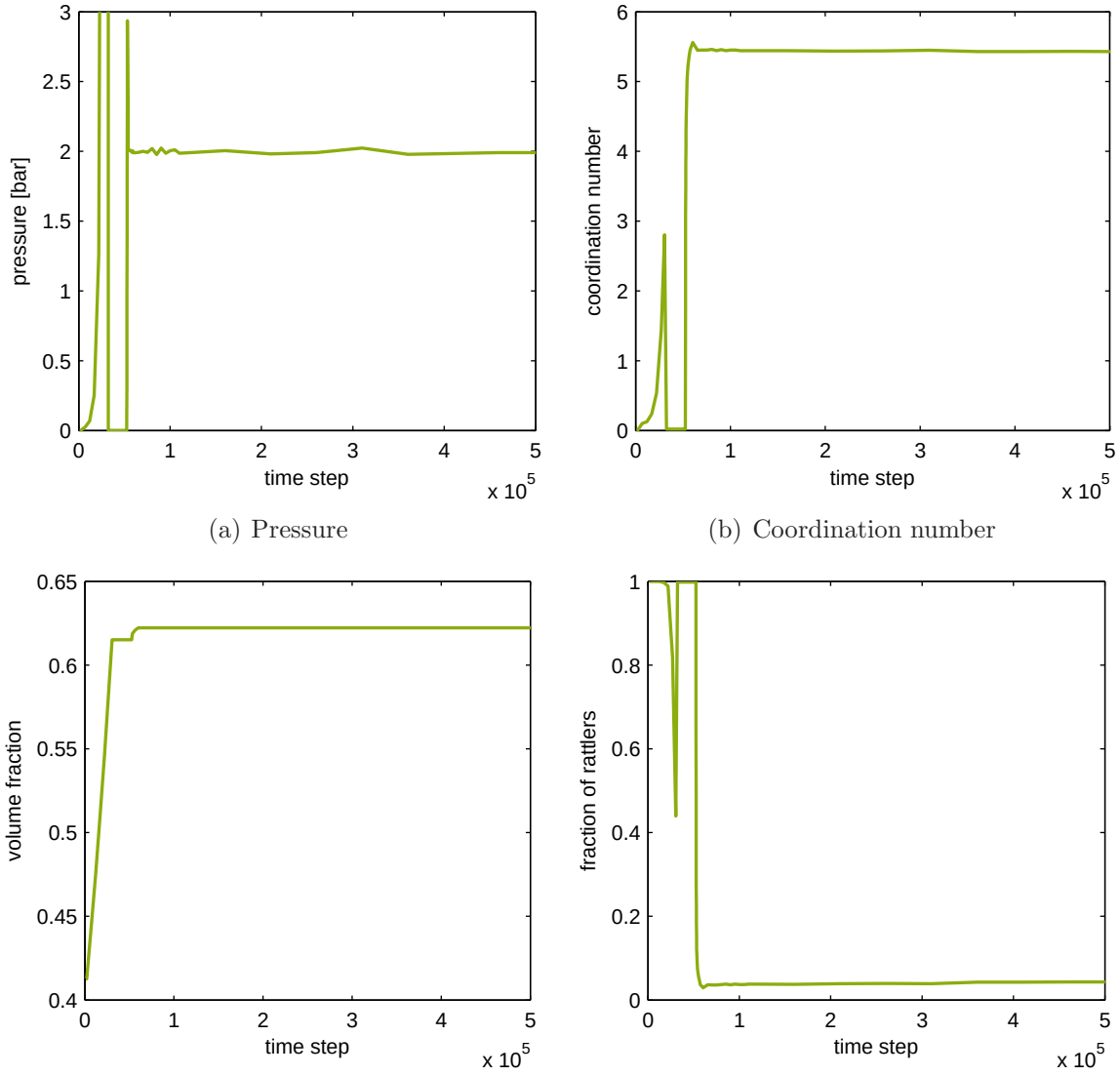

(a) Pressure

(b) Coordination number

(c) volume fraction

(d) number of rattlers

Figure 5.2: Initial state creation, Sample (1)

			Sample (1)	Sample (2)	Sample (3)
length in $\mathbf{e}_1$	$l_{\mathbf{e}_3}$	mm	6.23	6.23	6.23
length in $\mathbf{e}_2$	$l_{\mathbf{e}_2}$	mm	6.23	6.22	6.22
length in $\mathbf{e}_3$	$l_{\mathbf{e}_1}$	mm	32.37	32.40	32.36
pressure	p	bar	2.01	2.00	2.01
volume fraction	ψ		0.622	0.623	0.624
coordination number	Z		5.380	5.258	5.293
fraction of rattlers			0.050	0.058	0.06

Table 5.5: Simulation: initial states

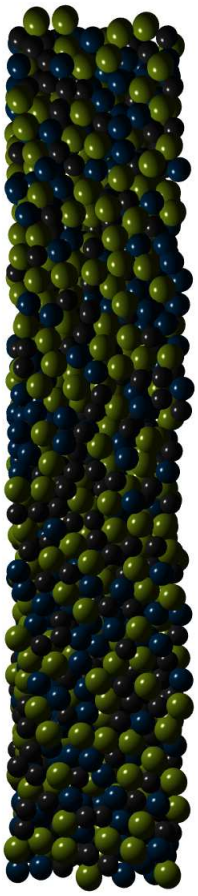

Figure 5.3: Initial state

5.4 Hooke's law

In the TRUBAL code a subroutine, called Probe, is implemented, which is comparable to the method **Hooke's law** used for the regular system (cf. chapter 3.3). The Probe command applies a small strain rate on all the particles in a required direction. The strain rates in the other directions are set to zero. Choosing the direction of applied strain rate in $\mathbf{e}_{33}$-direction, this equals the computation of the compressional modulus M, as explained in 2.1. With the command one needs to specify the number of time steps for which the strain is applied. The resulting strain $\Delta\varepsilon$ and the change in stress $\Delta\sigma$ is measured after relaxation of the system. The relation of change in stress and strain in

the same direction gives the compressional modulus M,

$$M = \frac{\Delta\sigma_{33}}{\Delta\varepsilon_{33}} \quad . \tag{5.6}$$

Since the system is in an isotropic stress state, the values for M in all three direction, $\mathbf{e}_1$, $\mathbf{e}_2$ and $\mathbf{e}_3$ should be the same. The compressional modulus is calculated for different number of time steps, at which the strain rate is applied. This number of time steps should not be chosen too high (≤ 30). The mean of the results are summarized in table 5.6, while the total results can be found in appendix A.1.

	v_P $[\frac{\mathrm{m}}{\mathrm{s}}]$	M [MPa]
Sample (1)	529.87 ± 1.38	436.77 ± 2.28
Sample (2)	524.44 ± 1.67	428.41 ± 2.73
Sample (3)	526.50 ± 0.82	432.45 ± 1.35
mean	526.94 ± 2.09	432.54 ± 4.06

Table 5.6: **Hooke's law** - Results

5.5 Wave propagation

In a similar way as for the regular system a simulation of a wave propagating through the system is conducted.

Since in a random system the particle layers are not as well defined as in a regular system, the first question is how to excite a wave. One idea is to excite a wave by point excitation, as thoroughly worked on in [21]. In this case just one particle is excited. Another idea, which is more similar to the excitation method in the regular systems, is to excite all the particles in a bin of two times the maximal particle radius. Because the system's boundary conditions are periodic in all directions, it is thought to be convenient to excite the waves at half the system's length. In this way two waves are propagating, one in $\mathbf{e}_3$-direction and one against this direction. Only the part of the system, where the wave

travels in excitation direction is taken into account. To produce more data and regard the full system once initial velocities in positive and once in negative $\mathbf{e}_3$-direction are used for wave excitation. As output for the wave analysis the position vector, the displacement vector and the velocity vector for every particle for every time step is requested. Other information, e.g. the pressure or the coordination number, are also available during the computation and can be requested as output, if needed.

The single particle excitation was not regarded a good method to obtain the P-wave speed. It is not clear which excitation particle to chose and which particles for the analysis of the travel time. The results do not give satisfying statistics comparing different particles. Another point is that no plane waves are excited. The magnitude of the velocities in wave excitation direction and in the shear directions cannot not be distinguished well. Furthermore, it was difficult to find the correct peak in the kinetic energy. The main reason for choosing a layer excitation however is the better similarity to the experiments. The ultrasonic transducer does not just excite a point, but a complete range of particles. In [21], the particle excitation is also chosen, because it is more similar to the experiments, that are supposed to be simulated.

For the layer excitation the magnitude of the excitation velocity is determined in the same way as for the regular systems. The velocity $v_0 = 3.16\,10^{-11}\frac{\mathrm{m}}{\mathrm{s}}$ is found to be small enough. How the wave propagates through the system, is visualized in figure 5.4, where the kinetic energy is plotted over time and initial particle position.
At the excitation layer around 0.015 mm from the sample's bottom, the peaks in kinetic energy are highest at the starting time, which is the time of excitation. They then reduce over time in this layer. Looking from this initial layer to the positions farther away from the source as time goes by the kinetic energy increases from zero to oscillating values. The wave has reached these parts. In comparison to the regular systems more fluctuations can be detected, but still a wave propagating over time from the excitation layer till the sample's end is visible.

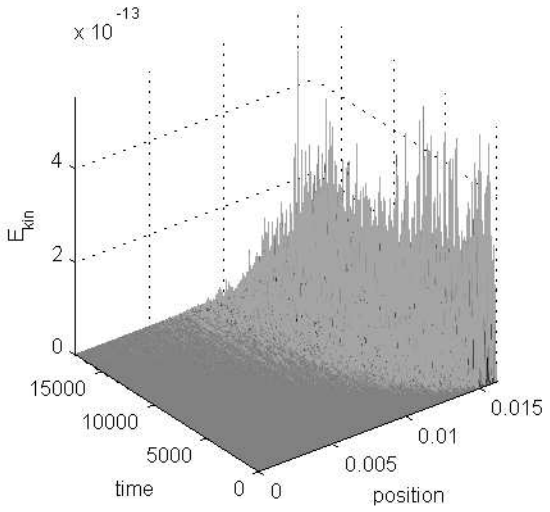

Figure 5.4: Kinetic energy over time and particle position of a downward propagating wave

Another way to look at the propagating wave is by looking at the single components of the velocity vector. The velocities for an excitation particle (cf. fig 5.5(a)), a particle close to the excitation layer (cf. fig 5.5(b)) and the velocities for a particle at the end of the sample (cf. fig. 5.5(c)) are plotted in figure 5.5. Note the different scaling of the velocity-axes, which is needed because of the different magnitudes of the values that are plotted.

In comparison to the regular systems, it is remarkable that the magnitudes of the velocities in wave propagation direction do not differ from the magnitudes of the other two velocity components. Due to the randomly sorted particles they excite oscillations in all directions with a similar intensity. Although the oscillations in wave propagation direction are not dominant in magnitude, they are the first ones to be noticed. So the first peak in kinetic energy over time is mainly influenced by the this velocity component. Apart from some small numerical influences one can also observe that the oscillations start in the excitation layer, while the velocities in the other layers are zero and start moving later in time as soon as the wave reaches this part of the system.

The wave speed can now be analysed by looking at the travel time t_s, which is the time, at which the first peak in kinetic energy occurs, for various single particles and their distance to the excitation source. To analyse the downward wave, particles with more than

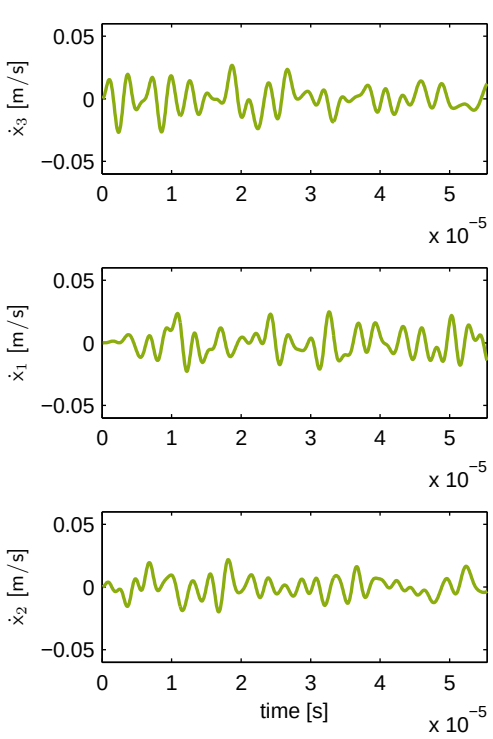

(a) Particle in excitation layer

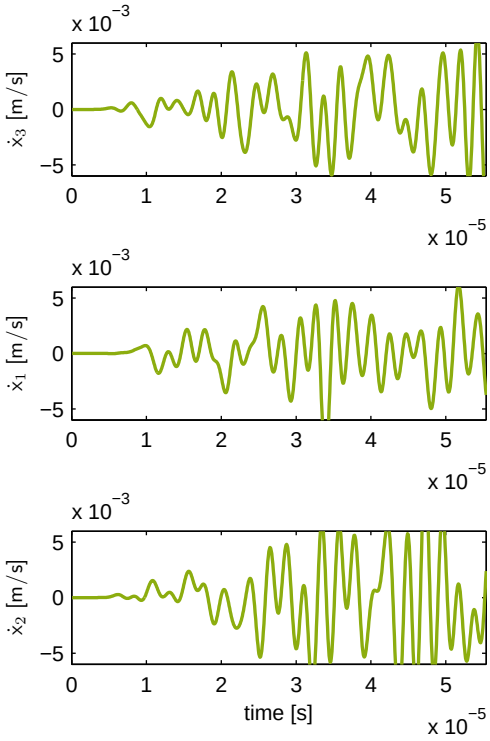

(b) Particle close to excitation layer

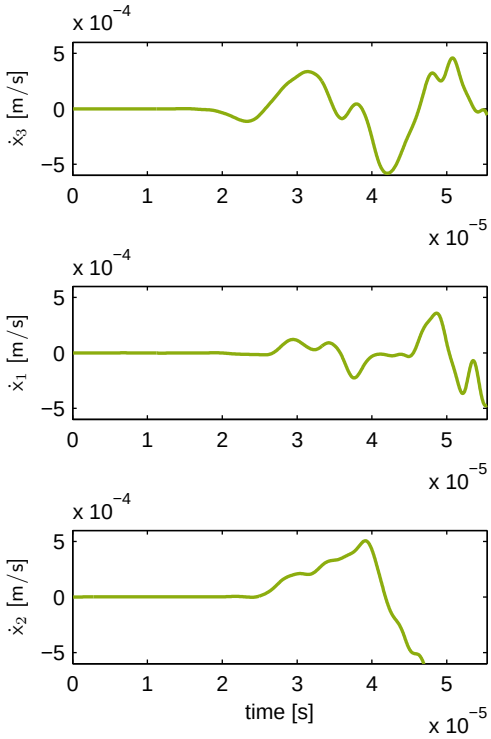

(c) Particle farther away

Figure 5.5: Velocity components

five contacts in the sample height of $\frac{0.5}{6}l_{\mathbf{e}_3}$, $\frac{1}{6}l_{\mathbf{e}_3}$, $\frac{1.5}{6}l_{\mathbf{e}_3}$ and $\frac{2}{6}l_{\mathbf{e}_3}$ are picked. The upward wave is analysed by particles with more than five contacts in the height of $\frac{4}{6}l_{\mathbf{e}_3}$, $\frac{4.5}{6}l_{\mathbf{e}_3}$, $\frac{5}{6}l_{\mathbf{e}_3}$ and $\frac{5.5}{6}l_{\mathbf{e}_3}$. Figure 5.6 shows a schematic of the system with the upward and downward wave and the heights at which the particles are evaluated. The distance to the excitation

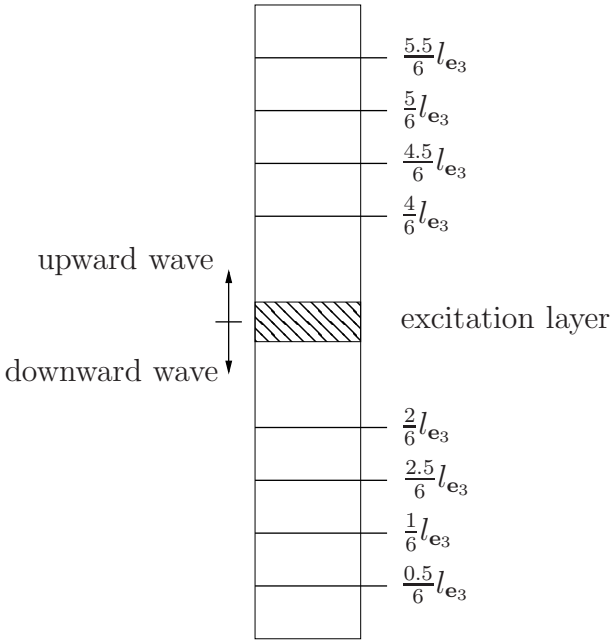

Figure 5.6: schematic of sample for wave propagation

source, which is the travel length l_{travel} of the wave until it reaches the investigated particle p, is initially defined as

$$l_{\text{travel}} = \left| x_3^{(p)} - \frac{1}{2}l_{\mathbf{e}_3} \right| \quad . \tag{5.7}$$

So the middle of the excitation layer with a thickness of $2\,r_{\max}$ is taken. Other possibilities would be to choose the boundaries of the layer as reference height. The choice of the correct travel length is discussed later.

The wave velocity is calculated with all the picked particles, which are about four to eight per layer,according to equation (5.8).

$$v_P = \frac{l_{\text{travel}}}{t_s} \tag{5.8}$$

This is done for all the three created initial states with the results of the upward and downward wave propagation simulation. The results per particle can be found in ap-

pendix A.2. The data for the wave speeds is averaged in the different heights at which the particles are picked. Figure 5.7 shows the mean in wave speed and the deviation separated for each sample. The vertical line is positioned at half the system's length and indicates

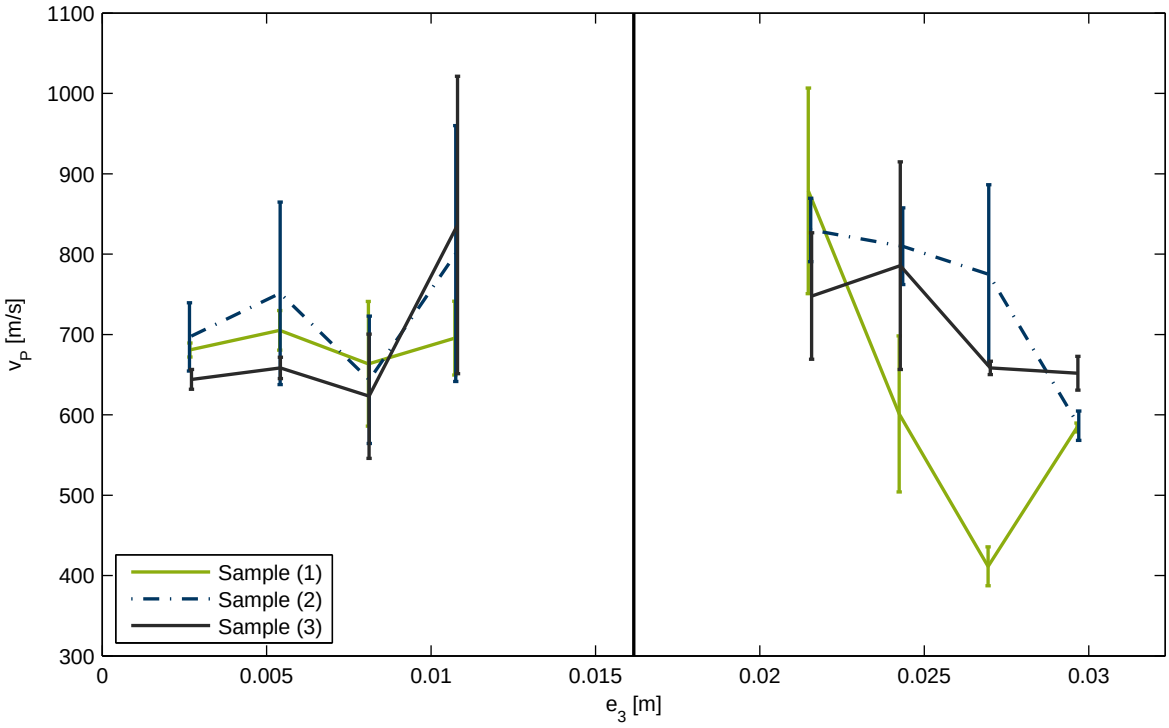

Figure 5.7: Statistics on the P-wave velocity per layer for all the samples

the wave excitation layer. The mean values vary from $623.12\frac{\mathrm{m}}{\mathrm{s}}$ to $836.23\frac{\mathrm{m}}{\mathrm{s}}$ for the downward wave and from $411.41\frac{\mathrm{m}}{\mathrm{s}}$ to $878.74\frac{\mathrm{m}}{\mathrm{s}}$ for the upward wave. The deviations closer to the excitation layer are bigger than at the farthest end of the sample for both waves. One reason for this could be that the wave is formed better after some time. Another reason lies in the method itself. The error due to the distance l_{travel} is higher closer to the excitation layer. It is also more difficult to specify the first peak in kinetic energy closer to the source. While most of the kinetic energy versus time plots for the particles far away from the source looked like figure 5.8(b), the plots for the particles close to the source are represented in figure 5.8(a). Note the different scaling of the kinetic energy axis. The first peak in kinetic energy in 5.8(a) is evaluated at $t = 0.53\,10^{-5}$ s, while the second peak at $t = 0.72\,10^{-5}$ s would give values closer to the mean. Thus it is not clear whether the first peak is actually the correct peak to be chosen or whether the first bigger peak gives

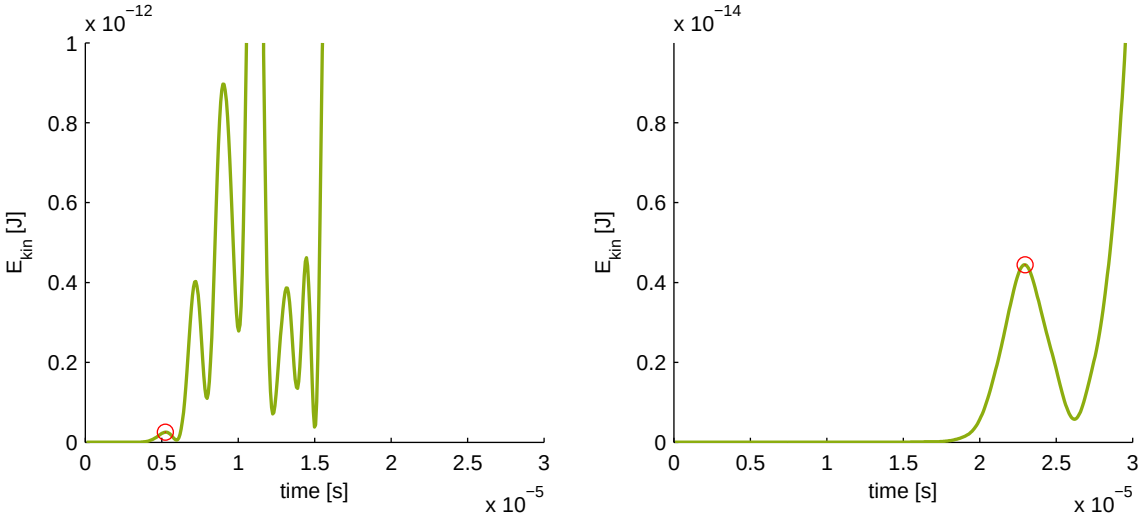

(a) Particle at $\frac{4}{6}l_{\mathbf{e}_3}$ (b) Particle at $\frac{5.5}{6}l_{\mathbf{e}_3}$

Figure 5.8: Kinetic energy over time for one particle for the upward wave of Sample (1)

better values. For particles farther away from the source, this problem vanishes. Almost all the plots are as clean as 5.8(b). A reason for this could be the frequency filtering phenomenon, that is stated in [17]. It is shown that the higher the polydispersity the more pronounced the filtering of frequencies get. The higher frequencies are trapped near the source and are not transmitted very far through the sample. Hence, the signal, measured in the form of kinetic energy, contains more frequencies near the excitation layer and is thus not very smooth. This effect can for example be reduced by exciting the wave in a different way with a better control of the frequency. A so called Ricker-wavelet, which is also supported in MATLAB (cf. [1]) and is characterized by one dominant frequency, could be possible solution. It is already used for the numerical simulation of waves in [9]. However, here different numerical algorithms are used to describe wave propagation.

An idea to eliminate the insecurity about the distance l_{travel} is realized by plotting the position in $\mathbf{e}_3$-direction of the picked particles versus the corresponding travel times t_s. The slope of a linear fitting curve gives the wave velocity. Figure 5.9 shows these aspects for the upward and downward wave. The fitting curves are created for each sample separately and once for the complete set of data (cf. tab. 5.7) The results of the linear fitting are in general lower than the first results, which indicates that the travel length is initially chosen to big. It would thus be more appropriate to chose the boundaries of

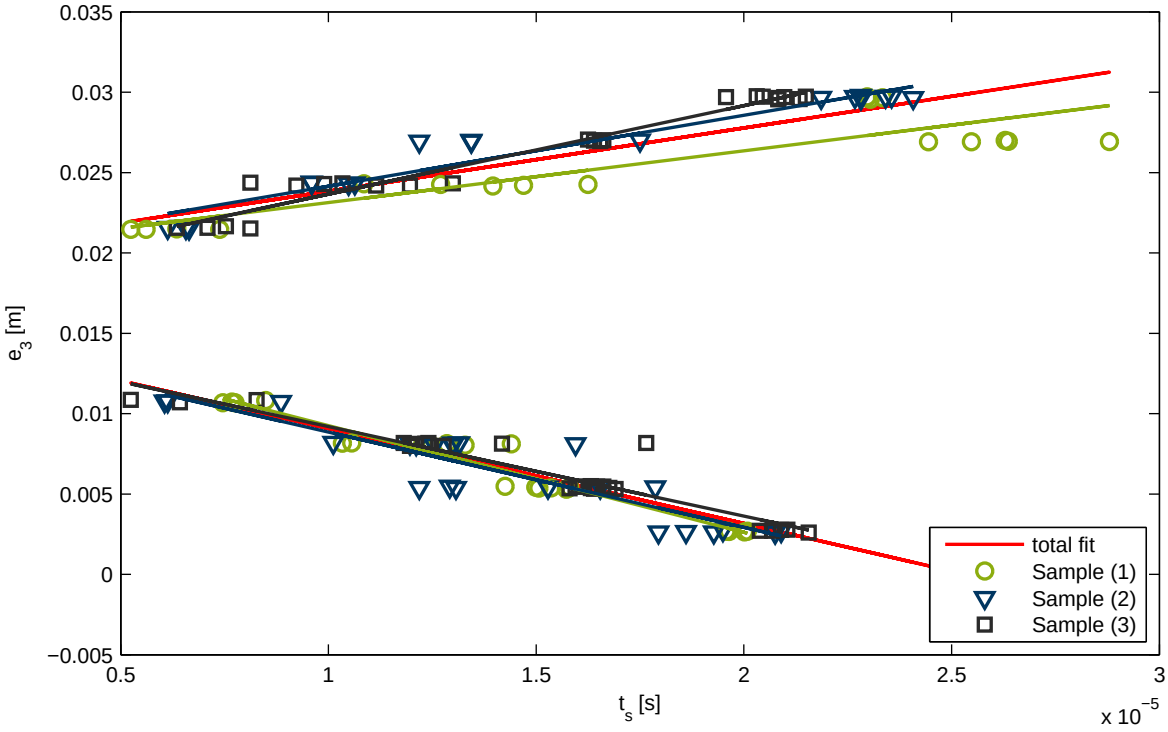

Figure 5.9: Statistics: travel time

	v_P $[\frac{\mathrm{m}}{\mathrm{s}}]$		M [MPa]	
	upward wave	downward wave	upward wave	downward wave
Sample (1)	321.38	664.01	160.68	685.90
Sample (2)	441.10	592.60	303.07	547.01
Sample (3)	550.69	557.46	473.11	484.82
mean	393.84	592.04	298.48	569.61

Table 5.7: Wave velocities and compressional modulus after linear fitting

the excitation layer as reference height. For the downward wave this height would be at $\frac{1}{2}l_{\mathbf{e}_1} - r_{\max}$ and for the upward wave at $\frac{1}{2}l_{\mathbf{e}_1} + r_{\max}$. The averages of the wave speeds are summarized in table 5.8 and the compressional moduli added. Although the results of the linear fitting are still in general lower, the wave velocities with the corrected travel length are show a better agreement than the ones with the initially chosen travel length.

	v_P $\left[\frac{\mathrm{m}}{\mathrm{s}}\right]$		M [MPa]	
	upward wave	downward wave	upward wave	downward wave
Sample (1)	571.14 ± 162.74	642.28 ± 49.15	546.36 ± 320.42	645.32 ± 95.79
Sample (2)	678.34 ± 106.50	666.56 ± 96.48	733.44 ± 224.83	705.93 ± 204.49
Sample (3)	669.97 ± 85.37	629.44 ± 79.34	711.14 ± 199.02	627.56 ± 171.76
mean	642.37 ± 127.00	645.22 ± 78.41	667.67 ± 258.05	658.02 ± 166.20

Table 5.8: Wave velocities and compressional modulus with corrected travel length

5.6 Fourier transform

A Fourier transform with the wave propagation simulation's results is conducted with the intention to gain information about the dispersion relation of the random configuration and thus the wave velocities. For the this transform the velocities in wave propagation direction $\mathbf{e}_3$ are used as input. The velocities are chosen instead of the amplitude, because they gave smoother spectra. The amount of data can be varied and should give the same results. One could omit some data on time steps or data on particles. The data that is evaluated here, covers all the time steps and the particles in the upper half of the sample for the upward wave and in the lower half of the sample for the downward wave. They are sorted in a matrix by $\mathbf{e}_3$-position in the columns and by time step in the rows.

The axes are scaled similarly as for the regular systems. The frequency axis is analogously scaled by $\Delta\omega = \frac{2\pi}{T}$ and the wave number axis by $\Delta k = k_{\min}$, with $k_{\min} = \frac{2\pi}{L}$. The total simulation time T is not dependent on the real simulation time, but on the data that is used as input. The same holds for the length L, which is the maximal distance in $\mathbf{e}_3$-direction between all the used particles for the transform.

For random systems one does not expect to see curves as for the regular systems. Figure 5.10 shows representatively a ω-k-plot for the upward wave (cf. fig 5.10(a)) and of the downward wave (cf. fig 5.10(b)) of Sample (1).

The first thing that can be noticed is the resolution. The distances from one point to the next one on the k axis equals Δk, which has a value of around 388 m^{-1}. The step on the ω-axis is $\Delta\omega$ with $113 \cdot 10^6$ Hz.

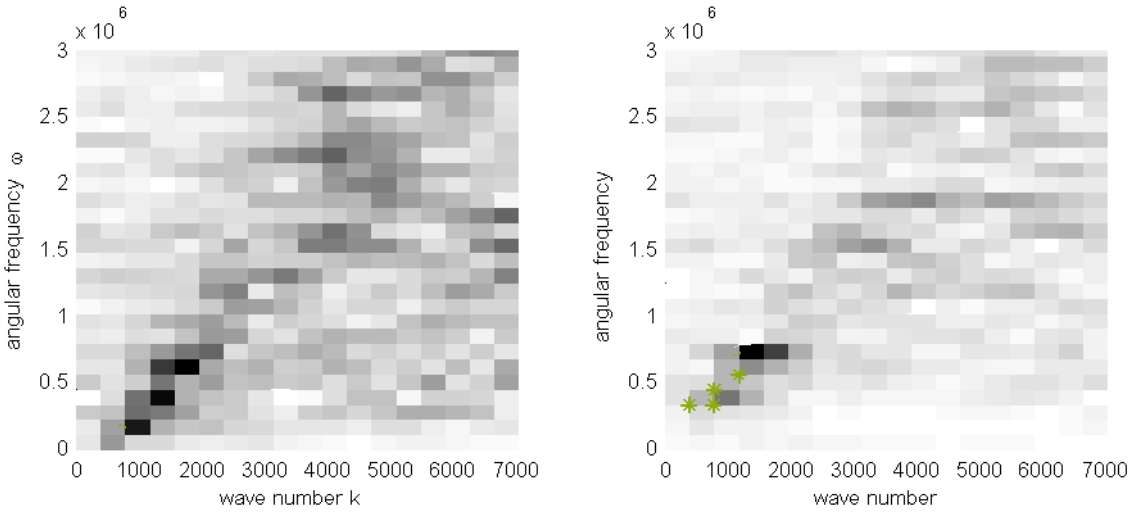

(a) upward wave (b) downward wave

Figure 5.10: Fourier transform Sample (1)

Figure 5.10(a) is chosen as an example which can be interpreted well. Overall the peaks do not follow a nice line but are completely smeared out. However for small wave numbers in the low frequency range, three higher peaks can be detected, which are aligned linearly. This is exactly the part, at which the slope gives the wave speed. With the coordinates of those peaks, the wave speed is computed.

Figure 5.10(b) is chosen as an example which cannot be interpreted well. Higher peaks in the lower frequency range cannot directly be identified. It is thus not well-defined how to calculate the wave speed.

The plots from in figure 5.10 can also be regarded from a different view-angle. This is shown in figure 5.11. The alternative view-angle makes it possible to have a better look at the peaks. The three peaks for the upward wave, that could already be identified in the 2D view, can now be visualized as well. They are marked with a green star (*). They are higher than all the other peaks in the plot and small of shape. There is no doubt in picking these peaks. For the downward wave there is one high peak. This peak is broader of shape. It is not clear which peaks in the surrounding area should be picked. Another point is that due to the relatively low resolution the actual highest point is probably not captured, because it could lie between two neighbouring points, thus differ between $\pm\Delta k$ and $\pm\Delta\omega$.

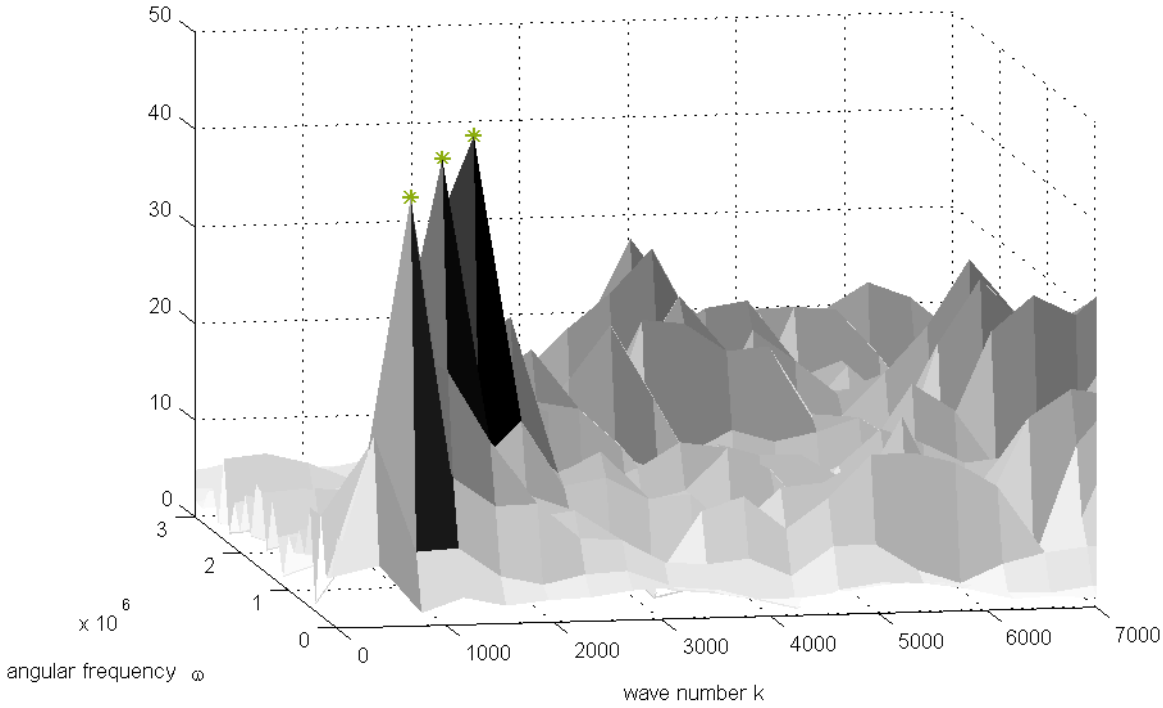

(a) upward wave

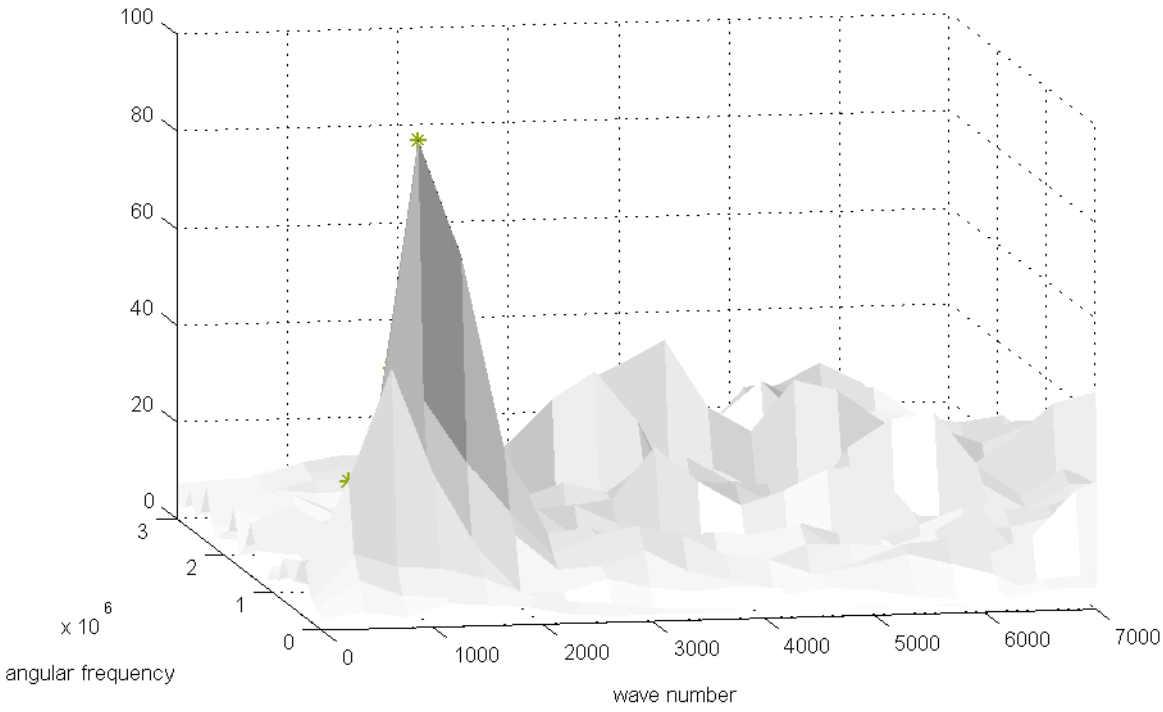

(b) downward wave

Figure 5.11: Fourier transform Sample (1) different view angle

The wave speeds are calculated for different possible choices of points for all the three samples for the upward and the downward wave. The results are given in appendix A.3

in dependency on the evaluated number of points. Only for the upward wave of sample (1) and the downward wave of sample (3) there is no doubt which peaks to pick. The wave speeds results in $583.15\frac{\mathrm{m}}{\mathrm{s}}$ (upward, sample (1)) and $581.71\frac{\mathrm{m}}{\mathrm{s}}$ (downward, sample (3)) with a compressional modulus of 529.01 MPa and 527.92 MPa, respectively. For the other samples the wave speeds vary from $291.84\frac{\mathrm{m}}{\mathrm{s}}$ to $132.49\frac{\mathrm{m}}{\mathrm{s}}$ with a compressional modulus from 132.49 MPa to 1196.7 MPa. Every sample and wave gives for a certain choice of points a wave speed around $580\frac{\mathrm{m}}{\mathrm{s}}$. The small differences in these values are due to the slightly different scaling. Δk differs for each sample, because the length of each sample is not determined to be completely equal. This means that exactly the same points are picked, which however results in a slight difference in wave speeds due to Δk.
The Fourier transform is expected to give better results by improving the resolution. This can be done by increasing the input data. One possibility to increase the input data is by running the simulation longer, which means a bigger total simulation time T and thus a smaller $\Delta\omega$. Another way is by creating a longer sample with more particles. This results in a longer L and thus a smaller Δk.

5.7 Comparison

Hooke's law, **wave propagation** and the **Fourier transform** are three different analysis methods which still should give the same material properties. Their orders of magnitude match, but their values differ from each other.
In contrast to the regular systems, where the **Wave propagation** method gave one result for each chosen method, the random system gives different results depending on the excitation layer and the chosen particles. In average these results are expected to give the wave speed of the sample. To obtain a reliable value different random samples need to be created and a lot of particles evaluated. The more data the better the statistics. Still there are some insecurities in averaging and especially in choosing the reference point from which the travel length is measured. The simulation itself is quick and unprob-

lematic, whereas the post-processing is a lot of work. The **Fourier transform** as as a post-processing method to analyse the wave speed, is a faster method. However the results deviate in about the same amount. **Hooke's law** gives the most consistent values. The experimentally obtained wave speeds lie approximately in the range of all the applied numerical methods.

All the three analysis methods serve as a good basis for future work, but need to be improved to obtain more consistent results. Different propositions for improvement have already been given in the according chapters and are again summarized in chapter 6. Then the simulation parameters, which are roughly estimated initially, can be matched better to the experimental setup.

Chapter 6

Conclusion and Outlook

This last chapter summarizes what has been investigated in this thesis and what is observed during the analysis. The main points in how the results are obtained are emphasized. The results are then and evaluated. Open questions are posed. Ideas and answers to these questions are given in the section Recommendations, stimulating possible future research on the subject.

6.1 Summary

In this thesis, the P-wave velocity and the compressional modulus are calculated by five different analysis methods for regular systems and by three different methods for a random system. Two of the methods are analytical. The numerical methods are based on the Discrete Element Method (DEM).

6.1.1 Regular Systems

As regular systems, four lattices are chosen: A simple cubic lattice and a hexagonally packed lattice in 2D and a simple cubic and a body-centred cubic (BCC) in 3D. They are frictionless and described by a linear contact model. The lattices are modelled as a simple mass-spring or mass-spring-dashpot system and code is realized during this thesis in MATLAB.

The five methods, that are used to calculate the wave velocity and the compressional modulus are the following:

Principle of virtual displacement

In this method the compressional modulus is directly calculated. A formula for the stiffness matrix is derived by the principle of virtual displacement.

Dispersion relation

The dispersion relation can be analysed by solving an eigenvalue problem that is obtained by combining the harmonic wave solution and wit Newton's equation of motion. It gives the angular frequency in dependency on the wave number. The slope at small wave numbers equals the wave velocity.

Hooke's Law

A DEM simulation is conducted with boundary and initial conditions, that allow to use the force-displacement relation for the calculation of the compressional modulus.

Wave propagation

A propagating wave is modelled in a DEM simulation. The wave is excited by an initial velocity for all the particles in a bottom layer. The initial velocity is chosen small enough to exclude the influence from this initial velocity on the wave propagation behaviour. As a result of this simulation, the kinetic energy over time is analysed to get information about the travel time and calculate with the travel distance the wave velocity.

Fourier transform

The results of the wave propagation simulations are analysed by a Fourier transform, which gives the dispersion relation and allows to calculate the wave velocity in the same way as mentioned above.

The results give one result for the wave velocity and the compressional modulus, which can easily be reproduced. The following important points can be observed:

- a good agreement in the results between all the methods for all the different lattices
- the **Fourier transform** produces the same graphs as obtained by the **Dispersion relation**

The evaluation of all the methods and especially the comparison of the three methods, that are based on simulations, with the analytical methods, confirm that each one of the methods is reliable. The study of the regular systems can thus serve as a validated basis for the disordered system.

6.1.2 Disordered system

The disordered system models experiments on ultrasonic wave propagation in a triaxial cell filled with glass bead, which are conducted in the Ruhr-University Bochum. For the DEM simulations the particle properties are chosen according the glass beads used in experiments. The system is frictional and described by a Hertzian contact model. The code used for the simulations is a Fortran code called TRUBAL. An initial packing of 2000 particles with three different radii is created, which represents an inner column of approximately one forth of the experimental setup's height.
Three of the analysis methods, that are used for the regular systems, can also be used for the disordered structure:

Hooke's law

TRUBAL provides a command that applies a strain rate on all the particles and measures the increment in stress. With the linear stress-strain relation the compressional modulus is calculated.

Wave propagation

A propagating wave is simulated in a DEM simulation. For the wave excitation an initial velocity of all the particles in a bin of two times the maximum particle radius is chosen. In the same way as for the regular systems, the initial velocity is chosen small enough to exclude the influence from this initial velocity on the wave propagation behaviour. The kinetic energy over time is evaluated to analyse the travel time and thus obtain the wave speed.

Fourier transform

The results of the wave propagation simulation are used as input for the Fourier transform. The transform is not expected to give the dispersion relation as nicely as for the regular systems, but still give information that can be used for the calculation of the wave velocity.

In contrast to the regular systems, the results for the random system are scattered and dependent on various different factors. They have to be analysed in a way, that requires a big amount of data to get meaningful statistics for the results. Therefore three different states are created with the same properties, but different random initial particle positions. They also show a different behaviour in the results:

- **Hooke's law** produces results with the smallest deviation in comparison to the other methods
- the results from the **Fourier transform** vary widely with high deviations
- the results for the **Wave propagation** vary widely with high deviations

- the experimental results lie in the upper range of the results obtained by the other methods

The questions that arouse during the analysis of the random system concern mainly the post processing step of the **Wave propagation** simulation, which is the main focus in this thesis.

- which constraints should be fulfilled for a particle to analyse?
- which reference height is the right one to choose for the calculation of the travel length?
- is the first peak in kinetic energy a good way to determine the travel time?

In this work all the particles in four different heights with more than five contacts are chosen to be analysed. In the same way as for the regular system the first peak in kinetic energy of one particle plotted over time is chosen as an indication for the travel time. The travel distance to calculate the wave speed is decided to be the distance from the chosen particle to the upper boundary of the excitation layer.

6.2 Recommendations

Some ideas, that might help answer the previously posed questions are given. These can be understood as recommendations for future work.
The initial choice of analysing only the particles with more than five contacts can be improved. Geometrically it makes more sense to look where the contacts are. For each particle, the neighbouring particles should be distributed in such a way, that the grant the mechanical stability of the particle. This is for example realized if the contact points form a tetrahedron. It is also well known, that in granular material the load, that is applied

at the boundaries is transmitted throughout the bulk following the paths designed by so-called force chains. They are for example defined in [22]. Similarly, it is assumed that waves tend to propagate preferably along these force chains. The motion is transferred faster and better along such chains. Therefore it would make sense to chose particles in such a chain. If the average of contact forces per particle is the higher than the total average of all contact forces, it is assumed that the particle is situated in a force chain. This could be checked, before analysing the chosen particle.

The question about the correct travel length, is investigated in this thesis. One way not having to determine this travel length is by calculating the slope of a linear fit of a travel time versus particle position plot. This method could be improved by increasing the statistics. Another way to reduce the influence of the error in the choice of travel length is creating a longer system. The longer the system, the lower the error in the chosen length.

A way to determine the travel time is investigated for the regular lattices. The peak in kinetic energy is found to be a good method for the regular systems. It is also preferred to choosing the amplitude in displacement for example. Before one would come up with a completely different method, this method can still be improved. As described in chapter 5.5, it is not always clear to pick the right peak. The kinetic energy plots of the particles farther away from the source happen to be cleaner and their analysis easier. This could also be the reason for the lower deviations in the wave speeds calculated with particles farther away from the excitation layer. So if kinetic energy can in general be influenced to give smoother results, the general deviations in wave velocities are expected to decrease. It could be that the plots of the kinetic energy of particles near the excitation source are more difficult to interpret, because the frequencies are trapped near the source and only the low frequencies are transmitted. So the excitation of a wave, where the frequencies are controlled better, is considered to be a solution to this problem. The frequency of the wave can for example be controlled by using a Ricker-wavelet, as already proposed in chapter 5.5. It could be a good method for the purpose of smoothing out the kinetic energies.

Finally the **Fourier transform** is actually expected to give better results. A better algorithm must be developed for choosing the right peaks (cf. chapter 5.6). The main problem of the Fourier method is however thought to be the low resolution, which is not small enough to detect the the peaks correctly. With a higher resolution the evaluation of the peaks is expected to be easier. But more importantly, the neighbouring values come closer together, which should reduce the high deviations. This resolution can be improved by adding more data. A longer sample, with longer simulation times can be the solution. After all the methods are improved in the ways just proposed or by ideas, which have not been considered yet, the parameters need to be matched with the experiments in a better way. The friction coefficient or the Poisson's ratio still depend on an initial guess based on empirical knowledge. In this context, it makes however also sense to think about possible error sources in the experimental setup or the experimental data evaluation.
Generally all the methods cannot only be adapted to the calculation of the compressional modulus, but in the same way the S-wave velocity and the shear modulus can be analysed and used to validate the chosen methods. This is another challenge for future work. Additionally it was also found interesting to study the dependence of the wave speeds measured at different heights of the sample on the magnitude of the excitation velocity.

6.3 Final remarks

Concludingly one can state that five useful methods are developed and validated for the analysis of the P-wave velocity and the compressional modulus in regular granular structures. Three of them can be used for random systems. An improvement of these three methods is required to simulate experiments reliably and get better information and understanding on wave propagation in granular material. The simulation allows to get information about the internal structure of the material, which is not accessible in the experiments. Once the moduli between the experiments and the numerical analysis are matched, the system can be described more fully. The simulations can then also serve as

a faster and much cheaper method for parameter studies.

Appendix A

Random Configuration

A.1 Hooke's law results

N_T	M_{11} [MPa]	M_{22} [MPa]	M_{33} [MPa]	G [MPa]
10	434.59	437.12	437.12	184.71
15	435.7	439.29	439.29	183.37
18	436.18	438.94	438.94	183.56
20	433.15	438.74	438.74	184.94
22	432.36	439.54	439.54	184.45
24	434.27	437.73	437.73	184.84
26	432.96	436.57	436.57	184.99
28	433.15	438.25	438.25	184.89
30	433.55	437.19	437.19	185.44
mean	433.9918± 1.2974	438.152± 1.0535	438.152± 1.0535	184.576 ± 0.68332

Table A.1: Probe - Sample (1)

N_T	$M_{11}[MPa]$	M_{22} [MPa]	M_{33} [MPa]	G [MPa]
10	431.67	427.8	427.8	178.08
15	434.41	425.59	425.59	179.81
18	431.94	426.91	426.91	180
20	430.78	428.31	428.31	180.81
22	432.45	426.82	426.82	180.58
24	432.65	426.34	426.34	180.74
26	431.83	425.53	425.53	180.31
28	430.48	426.42	426.42	180.24
30	431.22	426.08	426.08	180.7
mean	431.9391± 1.1698	426.6429± 0.9384	426.6429± 0.9384	180.1395 ± 0.84692

Table A.2: Probe - Sample (2)

N_T	$M_{11}[MPa]$	M_{22}[MPa]	M_{33} [MPa]	G [MPa]
10	435.51	433.43	433.43	181.07
15	434.16	430.48	430.48	180.53
18	434.19	433.38	433.38	180.98
20	433.03	432.76	432.76	181.38
22	432.62	430.6	430.6	180.92
24	432.05	431.18	431.18	180.91
26	433.58	432.16	432.16	181.31
28	433.55	432.71	432.71	181.31
30	432.91	430.59	430.59	181.61
mean	433.5125± 1.0247	431.9224± 1.2212	431.9224± 1.2212	181.1141 ± 0.32417

Table A.3: Probe - Sample (3)

A.2 Wave propagation results

	x_1	x_2	x_3	t_s	v_P	$v_{P,\text{cor}}$
$\frac{4}{6}\, l_{\mathbf{e}_3}$	0.0033066	0.0030751	0.021492	6.3508e-006	839.24	767.75
	0.002474	0.0018795	0.021463	5.2431e-006	1010.9	924.41
	0.0056561	0.0030108	0.021472	7.3846e-006	718.93	657.56
	0.0017695	0.00078752	0.021471	5.6123e-006	945.87	865.03
MEAN	$\bar{x_3} = 0.021475$			$\bar{v_P} = 878.735 \pm 127.896$		
				$\bar{v}_{P,\text{cor}} = 803.6867 \pm 116.8811$		
$\frac{4.5}{6}\, l_{\mathbf{e}_3}$	0.0058547	0.0027258	0.024259	1.2702e-005	637.46	601.7
	0.00082842	0.0057284	0.024303	1.0855e-005	749.92	708.13
	0.0020854	0.001886	0.024262	1.6246e-005	498.55	470.63
	0.003689	0.005853	0.024199	1.4695e-005	546.88	516.01
	0.0029096	0.0049997	0.024161	1.3957e-005	573.06	540.57
MEAN	$\bar{x_3} = 0.024237$			$\bar{v_P} = 601.174 \pm 97.0978$		
				$\bar{v}_{P,\text{cor}} = 567.4097 \pm 91.7988$		
$\frac{5}{6}\, l_{\mathbf{e}_3}$	0.0050584	0.0060619	0.026939	2.6363e-005	408.79	391.56
	0.0045842	0.0022084	0.027004	2.6289e-005	412.41	395.14
	0.00052406	0.00047235	0.026926	2.88e-005	373.72	357.98
	0.0014241	0.0052303	0.026915	2.4443e-005	439.88	421.34
	0.0044399	0.0012681	0.02692	2.5477e-005	422.24	404.44
MEAN	$\bar{x_3} = 0.026941$			$\bar{v_P} = 411.408 \pm 24.2705$		
				$\bar{v}_{P,\text{cor}} = 394.0913 \pm 23.2434$		
$\frac{5.5}{6}\, l_{\mathbf{e}_3}$	0.0041459	0.00060038	0.029561	2.304e-005	581.52	561.84
	0.0036766	0.0037106	0.029648	2.3335e-005	577.89	558.47
	0.0027817	0.0036621	0.029703	2.2966e-005	589.59	569.83
	0.00024578	0.0015698	0.029663	2.2966e-005	587.84	568.09
MEAN	$\bar{x_3} = 0.029644$			$\bar{v_P} = 584.21 \pm 5.4559$		
				$\bar{v}_{P,\text{cor}} = 564.5579 \pm 5.3173$		

Table A.4: Upward wave - Sample (1)

	x_1	x_2	x_3	t_s	v_P	$v_{P,\mathrm{cor}}$
$\frac{2}{6}\, l_{\mathbf{e}_3}$	0.0058002	0.0061212	0.010716	7.68e-006	709.23	638.05
	0.0018606	0.0057239	0.010819	8.4923e-006	629.23	564.89
	0.00052163	0.00023474	0.010676	7.4585e-006	735.6	662.36
	0.0057396	0.0050774	0.010677	7.7539e-006	707.49	637
MEAN	$\bar{x_3} = 0.010722$			$\bar{v_P} = 695.3875 \pm 45.9418$		
				$\bar{v}_{P,\mathrm{cor}} = 625.5723 \pm 42.1184$		
$\frac{1.5}{6}\, l_{\mathbf{e}_3}$	0.0043939	0.0012096	0.0081578	1.0338e-005	774.27	721.45
	0.0027645	0.0026547	0.0081297	1.2849e-005	625.16	582.65
	0.0037533	0.0056095	0.00812	1.44e-005	558.51	520.57
	0.0036212	0.0020968	0.0080177	1.2258e-005	664.42	619.88
	0.00075255	0.00062613	0.0080348	1.3292e-005	611.46	570.37
	0.0046216	0.00034852	0.0080021	1.248e-005	653.88	610.1
	0.0011798	0.0042955	0.0081783	1.056e-005	756.08	704.35
MEAN	$\bar{x_3} = 0.0080915$			$\bar{v_P} = 663.3971 \pm 77.6052$		
				$\bar{v}_{P,\mathrm{cor}} = 618.4831 \pm 72.1496$		
$\frac{1}{6}\, l_{\mathbf{e}_3}$	0.0044888	0.0047524	0.0054236	1.4991e-005	716.37	679.91
	0.0025635	0.0038695	0.0053718	1.5065e-005	716.3	680.01
	0.0012382	0.0023901	0.0053874	1.5803e-005	681.84	647.27
	0.0060436	0.0041331	0.0052987	1.5729e-005	690.68	655.95
	0.0051953	0.0054811	0.0053865	1.536e-005	701.56	666
	0.00089336	0.00077302	0.0054772	1.4252e-005	749.73	711.41
	0.0058516	0.0016394	0.0054206	1.5803e-005	679.73	645.17
MEAN	$\bar{x_3} = 0.0053951$			$\bar{v_P} = 705.1729 \pm 24.6623$		
				$\bar{v}_{P,\mathrm{cor}} = 669.3893 \pm 23.2997$		
$\frac{0.5}{6}\, l_{\mathbf{e}_3}$	0.0024327	0.0032281	0.0026813	2.0086e-005	671.17	643.98
	0.00264	0.0022556	0.0026628	1.9643e-005	687.25	659.44
	0.0020039	0.001438	0.0026452	2.0012e-005	675.45	648.16
	0.0024773	0.0053741	0.0026794	1.9569e-005	689	661.09
MEAN	$\bar{x_3} = 0.0026672$			$\bar{v_P} = 680.7175 \pm 8.7593$		
				$\bar{v}_{P,\mathrm{cor}} = 653.1661 \pm 8.3987$		

Table A.5: Downward wave - Sample (1)

	x_1	x_2	x_3	t_s	v_P	$v_{P,\text{cor}}$
$\frac{4}{6}\, l_{\mathbf{e}_3}$	0.0054096	0.0022245	0.021528	6.6462e-006	801.84	727.03
	0.0014182	0.0037758	0.021562	6.1292e-006	874.96	793.9
	0.0044731	0.001852	0.021544	6.5723e-006	813.25	737.64
MEAN	$\bar{x_3} = 0.021545$			$\bar{v_P} = 830.0167 \pm 39.338$		
				$\bar{v}_{P,\text{cor}} = 752.8593 \pm 35.9399$		
$\frac{4.5}{6}\, l_{\mathbf{e}_3}$	0.0055493	0.00068404	0.024357	9.6e-006	849.74	798.02
	0.00076155	0.0019464	0.024306	1.0486e-005	773.08	725.73
	0.0044771	0.0048582	0.024325	1.0634e-005	764.14	717.42
	0.00080453	0.0038646	0.02438	9.6e-006	852.2	800.42
MEAN	$\bar{x_3} = 0.024342$			$\bar{v_P} = 809.79 \pm 47.701$		
				$\bar{v}_{P,\text{cor}} = 760.3957 \pm 44.9679$		
$\frac{5}{6}\, l_{\mathbf{e}_3}$	0.0034546	0.0014434	0.026932	1.344e-005	798.57	761.61
	0.0055185	0.0057593	0.026933	1.2185e-005	880.96	840.13
	0.0045579	0.0047423	0.027002	1.7502e-005	617.27	588.85
	0.0024937	0.0021042	0.026979	1.344e-005	802.06	765.1
MEAN	$\bar{x_3} = 0.026961$			$\bar{v_P} = 774.715 \pm 111.6449$		
				$\bar{v}_{P,\text{cor}} = 738.9224 \pm 106.4048$		
$\frac{5.5}{6}\, l_{\mathbf{e}_3}$	0.0023902	0.0020255	0.029618	2.2818e-005	588.09	566.31
	0.0047406	0.0022192	0.029708	2.2671e-005	595.87	573.95
	0.0012653	0.0039918	0.02974	2.3557e-005	574.84	553.72
	0.0034316	0.0033072	0.029724	2.3409e-005	577.76	556.54
	0.0058417	0.00012106	0.029641	2.4074e-005	558.37	537.72
	0.0037747	0.0013483	0.029777	2.2818e-005	595.02	573.28
	0.0053644	0.0015635	0.029654	2.1858e-005	615.53	592.83
MEAN	$\bar{x_3} = 0.029695$			$\bar{v_P} = 586.4971 \pm 18.2998$		
				$\bar{v}_{P,\text{cor}} = 564.9049 \pm 17.6433$		

Table A.6: Upward wave - Sample (2)

	x_1	x_2	x_3	t_s	v_P	$v_{P,\text{cor}}$
$\frac{2}{6}\, l_{\mathbf{e}_3}$	0.0048772	0.0025972	0.01073	8.8615e-006	617.15	560.4
	0.0032127	0.0039673	0.010754	6.0554e-006	899.25	816.13
	0.0059667	0.0013324	0.010771	6.1292e-006	885.63	803.53
MEAN	$\bar{x_3} = 0.010752$			$\bar{v_P} = 800.6767 \pm 159.0846$		
				$\bar{v}_{P,\text{cor}} = 726.6878 \pm 144.1457$		
$\frac{1.5}{6}\, l_{\mathbf{e}_3}$	0.0060887	0.0036171	0.0081632	1.3145e-005	611.34	573.05
	0.0014846	0.0043011	0.0081891	1.0117e-005	791.74	742.01
	0.0043033	0.00082699	0.0081518	1.2997e-005	619.17	580.46
	0.0024581	0.004352	0.0081089	1.2111e-005	668.01	626.46
	0.0042012	0.0061549	0.0081402	1.1963e-005	673.64	631.6
	0.0034087	0.00089244	0.0081098	1.5951e-005	507.14	475.59
	0.00090444	0.00090236	0.0080532	1.2554e-005	648.87	608.79
	0.00062787	0.0057434	0.0080371	1.2997e-005	627.99	589.28
MEAN	$\bar{x_3} = 0.0081192$			$\bar{v_P} = 643.4875 \pm 79.259$		
				$\bar{v}_{P,\text{cor}} = 603.4064 \pm 74.2095$		
$\frac{1}{6}\, l_{\mathbf{e}_3}$	0.0025265	0.0039345	0.0054675	1.2923e-005	830.42	791.5
	0.0037005	0.0039111	0.0053843	1.2185e-005	887.57	846.26
	0.0049569	0.004296	0.0053804	1.3071e-005	827.7	789.2
	1.6876e-006	0.0049657	0.0054019	1.5286e-005	706.34	673.43
	0.0003966	0.0057777	0.0054039	1.6542e-005	652.61	622.18
	0.0055873	0.0014581	0.0054273	1.7871e-005	602.76	574.6
MEAN	$\bar{x_3} = 0.0054109$			$\bar{v_P} = 751.2333 \pm 113.5708$		
				$\bar{v}_{P,\text{cor}} = 716.1949 \pm 108.2895$		
$\frac{0.5}{6}\, l_{\mathbf{e}_3}$	0.0019392	0.0015544	0.0027469	1.9495e-005	690.01	664.23
	0.0057418	0.0011654	0.0026026	2.0751e-005	655.23	630.98
	0.0052117	0.0049124	0.0026994	2.0898e-005	645.96	621.91
	0.0026263	0.0039615	0.002644	1.8609e-005	728.4	701.38
	0.0033483	0.0045145	0.002618	1.7945e-005	756.83	728.78
	0.0018067	0.0041781	0.0026078	1.9274e-005	705.16	679.06
MEAN	$\bar{x_3} = 0.0026531$			$\bar{v_P} = 696.9317 \pm 42.499$		
				$\bar{v}_{P,\text{cor}} = 671.0555 \pm 40.9504$		

Table A.7: Downward wave - Sample (2)

	x_1	x_2	x_3	t_s	v_P	$v_{P,\text{cor}}$
$\frac{4}{6}\, l_{\mathbf{e}_3}$	0.0024416	0.0027209	0.021515	8.1231e-006	657.18	595.77
	0.00081993	0.0026618	0.021557	6.3508e-006	847.17	768.64
	0.0016158	0.0031818	0.021559	7.0892e-006	759.17	688.86
	0.00018789	0.00020821	0.02166	7.5323e-006	727.87	661.75
MEAN	$\bar{x_3} = 0.021573$			$\bar{v_P} = 747.8475 \pm 78.7673$		
				$\bar{v}_{P,\text{cor}} = 678.7571 \pm 71.549$		
$\frac{4.5}{6}\, l_{\mathbf{e}_3}$	0.00057629	0.0041317	0.024193	1.1151e-005	718.9	674.15
	0.0061672	0.0031806	0.024331	1.2997e-005	627.39	589.02
	0.00055031	0.0013798	0.024335	1.0338e-005	789.08	740.91
	0.0053027	0.004744	0.024364	8.1231e-006	1007.9	946.5
	0.0051867	0.0034291	0.024193	1.1963e-005	670.03	628.4
	0.0030762	0.0059077	0.024185	9.2308e-006	867.49	813.53
	0.0054987	0.0056237	0.024284	9.8954e-006	819.23	768.89
MEAN	$\bar{x_3} = 0.024269$			$\bar{v_P} = 785.7171 \pm 129.1653$		
				$\bar{v}_{P,\text{cor}} = 737.3423 \pm 121.3945$		
$\frac{5}{6}\, l_{\mathbf{e}_3}$	0.00030581	0.0036017	0.027056	1.6246e-005	669.62	638.96
	0.0030531	0.0019905	0.027019	1.6615e-005	652.51	622.54
	0.00012998	0.0045705	0.026959	1.6542e-005	651.82	621.66
	0.0046634	0.0017799	0.026986	1.6394e-005	659.32	628.92
MEAN	$\bar{x_3} = 0.027005$			$\bar{v_P} = 658.3175 \pm 8.2603$		
				$\bar{v}_{P,\text{cor}} = 628.0191 \pm 7.9773$		
$\frac{5.5}{6}\, l_{\mathbf{e}_3}$	0.0026847	0.00050291	0.029754	2.0308e-005	668.57	644.01
	0.0029416	0.0055611	0.029695	2.0972e-005	644.55	620.8
	0.002076	0.0038824	0.029564	2.0825e-005	642.84	618.9
	0.0057697	0.0013104	0.029578	2.1342e-005	627.92	604.56
	0.0040335	0.00069492	0.02969	1.9569e-005	690.5	665.06
	0.0036379	0.004915	0.029719	2.1489e-005	630.17	606.98
	0.0011603	0.0040957	0.029721	2.0455e-005	662.11	637.77
	0.00041773	0.0010841	0.029644	2.0825e-005	646.69	622.74
MEAN	$\bar{x_3} = 0.029671$			$\bar{v_P} = 651.6688 \pm 20.9835$		
				$\bar{v}_{P,\text{cor}} = 627.6013 \pm 20.2733$		

Table A.8: Upward wave - Sample (3)

	x_1	x_2	x_3	t_s	v_P	$v_{P,\text{cor}}$
$\frac{2}{6}\, l_{\mathbf{e}_3}$	0.00035306	0.0054536	0.010849	8.2708e-006	644.2	583.56
	0.0050077	0.0030972	0.010863	5.2431e-006	1013.5	917.87
	0.0057348	0.0036011	0.01071	6.4246e-006	850.98	772.89
MEAN	$\bar{x_3} = 0.010807$			$\bar{v_P} = 836.2267 \pm 185.0915$		
				$\bar{v}_{P,\text{cor}} = 758.1069 \pm 167.6465$		
$\frac{1.5}{6}\, l_{\mathbf{e}_3}$	8.3093e-005	0.0014782	0.0080006	1.2775e-005	640.02	600.77
	0.0009802	0.0059158	0.0081742	1.2406e-005	645.08	604.65
	0.0047478	0.0010427	0.0081808	1.1815e-005	676.77	634.34
	0.0028919	0.0016711	0.0079902	1.1963e-005	684.35	642.42
	0.0028637	0.0048291	0.0081307	1.4178e-005	567.51	532.15
	0.00045032	0.0037085	0.0081719	1.7649e-005	453.57	425.16
	0.0037509	0.0010946	0.0081142	1.2111e-005	665.77	624.33
	0.0011545	0.0032339	0.0081378	1.2332e-005	651.89	611.23
MEAN	$\bar{x_3} = 0.0081125$			$\bar{v_P} = 623.12 \pm 77.3505$		
				$\bar{v}_{P,\text{cor}} = 584.382 \pm 72.6456$		
$\frac{1}{6}\, l_{\mathbf{e}_3}$	0.0059928	0.0012453	0.0053781	1.6763e-005	644.21	614.29
	0.0018985	0.001872	0.0053312	1.6394e-005	661.58	630.98
	0.0053518	0.0029809	0.0054529	1.6025e-005	669.23	637.92
	0.0032512	0.0049767	0.0054881	1.632e-005	654.96	624.23
	0.00090423	0.0051629	0.0053473	1.5803e-005	685.3	653.56
	0.0039869	0.0026502	0.0054682	1.6468e-005	650.3	619.83
	0.0036333	0.0035111	0.0053105	1.6911e-005	642.59	612.91
	0.0041313	0.0046336	0.0054678	1.6615e-005	644.54	614.37
	0.00071206	0.0013923	0.0054581	1.5951e-005	672	640.55
	0.0010457	0.0021667	0.0053677	1.632e-005	662.34	631.61
	0.0046108	0.0053379	0.0054896	1.632e-005	654.87	624.14
MEAN	$\bar{x_3} = 0.0054145$			$\bar{v_P} = 658.3564 \pm 13.3596$		
				$\bar{v}_{P,\text{cor}} = 627.6705 \pm 12.7556$		
$\frac{0.5}{6}\, l_{\mathbf{e}_3}$	0.00095597	0.005244	0.00278	2.1046e-005	636.56	612.73
	0.0034429	0.0024236	0.0027072	2.0677e-005	651.44	627.18
	0.0032652	0.0053406	0.002602	2.1563e-005	629.55	606.29
	0.0010373	0.0023944	0.0027626	2.0898e-005	641.89	617.9
	0.0026102	0.0020935	0.0027086	2.0382e-005	660.82	636.19
MEAN	$\bar{x_3} = 0.0027121$			$\bar{v_P} = 644.052 \pm 12.3173$		
				$\bar{v}_{P,\text{cor}} = 620.0604 \pm 11.8214$		

Table A.9: Downward wave - Sample (3)

A.3 Fourier transform results

upward wave		
number of points	v_P [$\frac{\text{m}}{\text{s}}$]	M [MPa]
3	583.15	529.01

downward wave		
number of points	v_P [$\frac{\text{m}}{\text{s}}$]	M [MPa]
2	291.84	132.49
2	583.68	529.97
2	583.68	529.97
2	875.51	1192.4
4	371.43	214.62
4	583.68	529.97
5	396.07	244.03

Table A.10: Fourier transform - Sample (1)

upward wave		
number of points	v_P [$\frac{\text{m}}{\text{s}}$]	M [MPa]
3	438.77	299.88
3	292.51	133.28
4	497.27	385.17
4	468.02	341.19
7	468.02	341.19

downward wave		
number of points	v_P [$\frac{\text{m}}{\text{s}}$]	M [MPa]
2	292.17	132.96
2	584.33	531.85
2	584.33	531.85
2	876.50	1196.7
4	584.33	531.85

Table A.11: Fourier transform - Sample (2)

upward wave		
number of points	v_P [$\frac{\text{m}}{\text{s}}$]	M [MPa]
2	292.11	133.12
2	438.17	299.53
2	584.23	532.50
3	438.17	299.53
4	438.17	299.53
5	438.17	299.53
5	563.37	495.14
6	549.86	471.69

downward wave		
number of points	v_P [$\frac{\text{m}}{\text{s}}$]	M [MPa]
5	581.71	527.92

Table A.12: Fourier transform - Sample (3)

Bibliography

[1] [2012]. 'http://www.mathworks.de/de/help/wavelet/ref/mexihat.html.'

[2] [October 2012]. 'http://www.mathworks.nl/help/matlab/ref/fft.html.'

[3] Albers, B. [April 2010]. *Modeling and Numerical Analysis of Wave Propagation in Saturated and Partially Saturated Porous Media (Veroffentlichungen Des Grundbauinstitutes Der Technischen Universitat Berlin)*. Shaker Verlag GmbH, Germany, first edition. ISBN 3832290087.

[4] Ashcroft, N. W. & D. N. Mermin [January 1976]. *Solid State Physics*. Brooks Cole, first edition. ISBN 0030839939.

[5] Chapman, C. [August 2004]. *Fundamentals of Seismic Wave Propagation*. Cambridge University Press. ISBN 052181538X.

[6] Cheeke, J. D. N. [April 2002]. *Fundamentals and Applications of Ultrasonic Waves (CRC Series in Pure and Applied Physics)*. CRC Press, first edition. ISBN 0849301300.

[7] Cundall, P. A. & O. D. L. Strack [January 1979]. 'A discrete numerical model for granular assemblies.' *Géotechnique*, **29**(1), pp. 47–65.

[8] Emmerich, S. [2012]. 'Cyclic triaxial tests to investigate ratcheting in granular media.' Ruhr-Universität Bochum.

[9] Frehner, M., S. M. Schmalholz, E. H. Saenger & H. Steeb [2008]. 'Comparison of finite difference and finite element methods for simulating two-dimensional scattering of elastic waves.' *Physics of the Earth and Planetary Interiors*, **171**(1-4).

[10] de Gennes, P. G. [March 1999]. 'Granular matter: a tentative view.' *Reviews of Modern Physics*, **71**(2), pp. S374–S382.

[11] Göncü, F. [2012]. *Mechanics of Granular Material: Constitutive Behavior and Pattern Transformation*. Ph.D. thesis, Technische Universiteit Delft.

[12] Jaeger, H. M., S. R. Nagel & R. P. Behringer [October 1996]. 'Granular solids, liquids, and gases.' *Reviews of Modern Physics*, **68**(4), pp. 1259–1273.

[13] Krause, M. [2012]. 'Realisierung einer drucksteuerung für eine triaxialzelle mit anschlie
ssender laufzeitbestimmung von glasperlenproben bei unterschiedlichen drücken.' Ruhr-Universität Bochum.

[14] Kruyt, N. P. [2010]. 'Three-dimensional lattice-based dispersion relations for granular materials.' In *IUTAM-ISIMM Symposium on Mathematical Modeling and Physical Instances of Granular Flows*, edited by J. Goddard, P. Giovine & J. T. Jenkins. AIP, Reggio Calabria (Italy), 14.18 September 2009.

[15] Le, K. C. [September 2011]. *Energy Methods in Dynamics (Interaction of Mechanics and Mathematics)*. Springer, 2012th edition. ISBN 3642224032.

[16] Luding, S. [October 2004]. 'Micro-macro transition for anisotropic, frictional granular packings.' *International Journal of Solids and Structures*, **41**(21), pp. 5821–5836.

[17] Luding, S. & O. Mouraille [2008]. 'Mechanic waves in sand: effect of polydispersity.' In *PARTEC 2007, Congress on Particle Technology*, edited by W. Peukert & C. Schreglmann. University of Erlangen-Nuremberg, Institute of Particle Technology.

[18] Maldovan, M. & E. L. Thomas [November 2008]. *Periodic Materials and Interference Lithography for Photonics, Phononics and Mechanics*. Wiley-VCH, first edition. ISBN 3527319999.

[19] Mouraille, O. [February 2009]. *Sound propagation in dry granular materials : discrete element simulations, theory, and experiments*. Ph.D. thesis, EMPTY, Enschede.

[20] Mühlmeier grinding GMBH [2008]. *Product information: MINIBEADS - glass beads*.

[21] O'Donovan, J., C. O'Sullivan & G. Marketos [October 2012]. 'Two-dimensional discrete element modelling of bender element tests on an idealised granular material.' *Granular Matter*, pp. 1–15.

[22] Radjai, F., D. E. Wolf, M. Jean & J.-J. Moreau [January 1998]. 'Bimodal Character of Stress Transmission in Granular Packings.' *Physical Review Letters*, **80**(1), pp. 61+.

[23] Rossing, T. D. [1990]. 'Laboratory observation of elastic waves in solids.' *American Journal of Physics*, **58**(12), pp. 1153+.

[24] Schnell, W., D. Gross & W. Hauger. *Technische Mechanik 2. Elastostatik*. Springer-Verlag GmbH, 6th edition. ISBN 3540641475.

[25] Song, C., P. Wang & H. A. Makse [May 2008]. 'A phase diagram for jammed matter.' *Nature*, **453**(7195), pp. 629–632.

[26] Stark, R. [August 2006]. *Festigkeitslehre: Aufgaben und Lösungen (German Edition)*. Springer, 2006th edition. ISBN 3211296999.